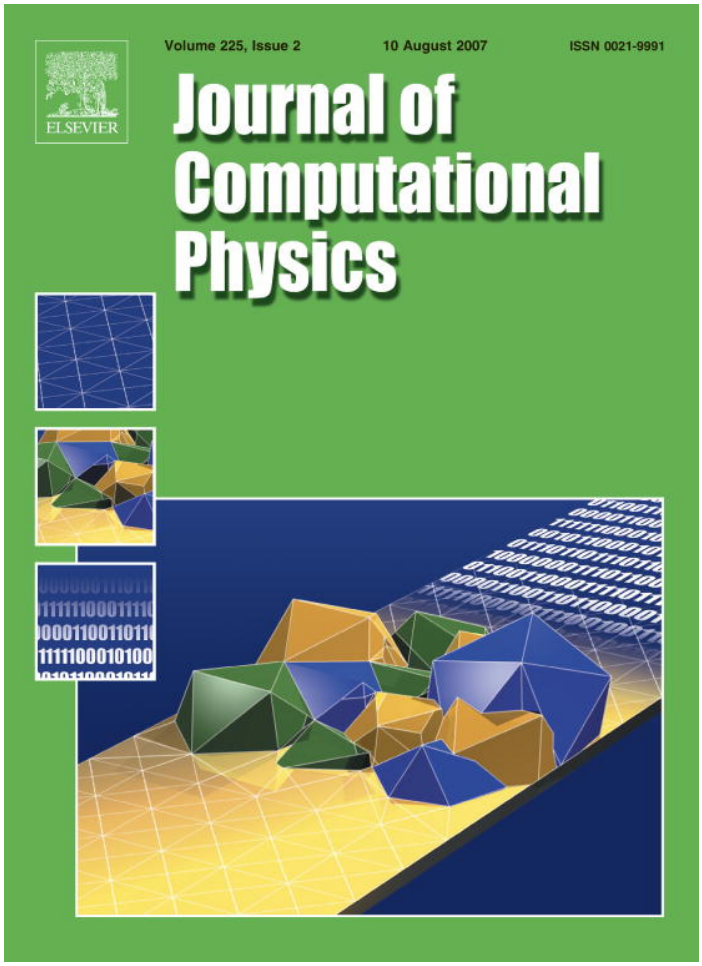

Available online at www.sciencedirect.com
ScienceDirect
Journal of Computational Physics 225 (2007) 1603–1631
JOURNAL OF COMPUTATIONAL PHYSICS
www.elsevier.com/locate/jcp

Mathematical modeling and simulation of aquatic and aerial animal locomotion

T.Y. Hou [a,*,1], V.G. Stredie [a], T.Y. Wu [b]

[a] *Applied and Computational Mathematics, Caltech, Pasadena, CA 91125, United States*
[b] *Division of Engineering and Applied Science, Caltech, Pasadena, CA 91125, United States*

Received 22 January 2006; received in revised form 13 December 2006; accepted 10 February 2007
Available online 24 February 2007

Abstract

In this paper, we investigate the locomotion of fish and birds by applying a new unsteady, flexible wing theory that takes into account the strong nonlinear dynamics semi-analytically. We also make extensive comparative study between the new approach and the modified vortex blob method inspired from Chorin's and Krasny's work. We first implement the modified vortex blob method for two examples and then discuss the numerical implementation of the nonlinear analytical mathematical model of Wu. We will demonstrate that Wu's method can capture the nonlinear effects very well by applying it to some specific cases and by comparing with the experiments available. In particular, we apply Wu's method to analyze Wagner's result for a wing abruptly undergoing an increase in incidence angle. Moreover, we study the vorticity generated by a wing in heaving, pitching and bending motion. In both cases, we show that the new method can accurately represent the vortex structure behind a flying wing and its influence on the bound vortex sheet on the wing.

PACS: 47.85.Gj; 47.32.C−; 47.15.Km

Keywords: Aerodynamics; Vortex dynamics; Potential flows

1. Introduction

The subject of animal locomotion has fascinated human minds for generations. Many experts have made important contributions to the theory of animal locomotion. Starting with the pioneering works of Sir James Gray (the Head of Cambridge University's Zoology Department, 1937–1961), the theory of animal locomotion stimulated Sir G.I. Taylor to make two important investigations, one involving the swimming of snakes and eels, while the other initiated hydrodynamic studies on ciliary propulsion. However, the main contributions to this field came later from Sir James Lighthill and Prof. Theodore Wu. Lighthill laid a theoretical

* Corresponding author.
E-mail addresses: hou@acm.caltech.edu (T.Y. Hou), gaby@acm.caltech.edu (V.G. Stredie), tywu@its.caltech.edu (T.Y. Wu).
[1] The research of T.Y. Hou was in part supported by a NSF FRG Grant No. DMS-0353838 and a NSF ITR Grant No. ACI-0204932.

0021-9991/$ - see front matter © 2007 Elsevier Inc. All rights reserved.
doi:10.1016/j.jcp.2007.02.015

foundation for the swimming of slender fish, while Wu made an extension of classical oscillating airfoil aerodynamics to a linear theory of flexible lifting-surface locomotion to examine the performance of bending wings of birds in flapping flight and the lunate tails of fast-swimming percomorph and acombroid fishes and rays in swimming.

There have been notable advances made in the field of unsteady wing theory and associated numerical methods in the past few decades. One of the pioneers in studies of wing in unsteady flight was Theodorsen with his theory of instability and the mechanism of flutter (see [27]). In 1931, Kaden introduced similarity variables for describing the roll-up of a semi-infinite plane vortex-sheet (see [24, p. 147]). During the 1950s, several authors presented approximate asymptotic solutions in which a two-dimensional spiral vortex generated behind a sharp edge was replaced by a single point vortex, an example of which is given by [23]. Moore in 1976 (see [16]) studied and verified the stability of a class of vortex sheets rolling-up, but could not verify the stability of the problem as noted later by Pullin in 1978 (see [22]), who obtained, for the first time, regular and well-defined starting vortex spirals from an accurate numerical solution of the Birkhoff–Rott equation (for inviscid flow) written in similarity variables. These results were used by Krasny to validate his method. In 1991 (see [11]), he provided an extensive discussion of Chorin's vortex blob method (see [2]) and applied it for the evolution of a free vortex sheet undergoing a certain perturbation and for the wake forming at the edges of a flat plate advancing broadwise perpendicular to the flow. Here, strong numerical evidence has been found indicating that the vortex blob method converges, even past the time then known for the critical vortex-sheet singularity formation, as the smoothing parameter tends to zero. Three years later, Sarpkaya (see [25]) published an excellent treatise on vortex dynamics, especially with viscous effects in various cases. More recently, in 2003, Jones (see [7]) analyzed a stalled airfoil held at a finite incidence angle for both edges sheding vortex sheets under two Kutta conditions, one at each edge.

There are many experiments reported in the fluid dynamics literature that are of help for verifying agreement with our computational results. Didden in 1979 (see [4]) performed an experiment in which a moving piston is used to force fluid out from a circular tube, leading to the formation of a vortex ring. The fluid mechanics literature is very rich in experiments on the performance of a heaving wing, as that conducted by Bratt in 1953 (see [1]) and more recently by Jones et al. in 1998 (see [6]) and by Lai et al. in 2002 (see [12]). For pitching, the experiment by Koochesfahani (see [10]) at Caltech for visualization of the wake behind a flat plate in pitching with various frequencies and pitching axes provided very useful information for the present comparative study.

Historically, pioneering development of linear unsteady airfoil theory dates back to Herbert Wagner [28] who was the first to have obtained an integral equation for calculating the wake vorticity shed by a wing. This approach was further developed by Kármán and Sears [8]. Its generalization to nonlinear theory was pursued earlier by McCune and co-workers (see [15]) but the full generalization to two-dimensional flexible lifting-surface performing arbitrary movements was done by Wu in 2001 (see [30]). Wu's method captures very well the nonlinear effects while the wake vorticity is being computed under the Kutta condition by Wu's generalized Wagner's integral equation for the conservation of total circulation.

The main objective of this paper is to develop a better method for capturing the nonlinear effects existing in highly nonlinear flow movements generated by bird's wing or fish fin. More specifically, strong nonlinear effects arise in general from changes in wing shape and from finite deviations in wing trajectory away from a rectilinear course, the former being local, bearing instantaneous effects, whereas the latter due to wing–wake interactions. These nonlinear effects are very important in cases involving irregular movements such as highly curved paths (e.g. quick U-turns). The main difficulty arises when analyzing the fluid properties near the trailing edge of a wing as well as the behavior of the flow with complicated distributions of vortices, both bound to the wing and free after being shed. These difficulties can be overcome by using Wu's method. The method will be applied to some significant cases and will be shown how well it matches the experimental data. Compared with other methods, Wu's method is found to be better in capturing the radius of a vortex forming behind a wing advancing with a sudden increase in the angle of attack. In Section 6, we will calculate the location of the core of the vortex ring by the modified vortex blob method and by Wu's method. We will see that the radii of the vortex rings are different, in Wu's method being 25% bigger than the vortex blob method. However, Wu's result agrees very well with the experiment in the sense that it verifies the square-root behavior of the radius versus Devenport's measurement [3].

Wu's method also shows more roll-ups inside the vortex ring compared to the vortex blob method. To get the same number of roll-ups for the vortex blob method, we will have to decrease the blob size and therefore to decrease the time step accordingly. This will increase considerably the total CPU time.

For nonlinear motions, Wu's method shows very good results when compared with the experiments for heaving and pitching. Some more interesting examples will be studied involving highly curved Heaviside, Fourier and bending motions. The lift and the thrust will be analyzed, emphasizing the effect of the free vortex sheet on a flying wing.

To further demonstrate that Wu's method captures the strong nonlinear effects, we apply Wu's method to reproduce Wagner's theoretical result. Wagner's theory applied to a forward flying wing with a Heaviside increase in angle of attack yields a stepwise gain of initial lift equal to half the asymptotic final lift. The result obtained by Wu's method is significantly better than that found in the literature (see [9]). We get a ratio of initial lift over final lift of about 0.64 while the result obtained by the vortex blob method is around 0.74, and that obtained by Katz and Plotkin in [9] is about 0.85.

We will try to demonstrate that all these improvements are due to the advantage of Wu's method in being able to capture more accurately the leading order effect of the very first vortex element shed from the wing's trailing edge. The error incurred in the first vortex element by any method (e.g. the vortex blob method) will propagate in the wake, causing more error in evaluating the bound vorticity at the wing, which in turn causing even more error in the next released free vortex at every time step; and this complex accumulation of error is the main source of discrepancies between the results obtained by these two differing approaches. A more detailed study of this 2D problem can be found in [26] and a simplified computational method for the 3D problem has been proposed and studied in detail in [5].

This paper is organized as follows. In Section 2, we will introduce Krasny's vortex-blob method. Krasny's ideas are taken from his papers of 1991 [11] and 1994 [21]. This method provides important insight for a number of fluid mechanics and numerical issues. Then we generalize some of these ideas to a flat plate moving broadwise perpendicular to the flow, hereby deriving a modified vortex blob method. In Section 3, we present Wu's theory for a flexible plate advancing at an angle of attack. Wu's theory was described in his 2001 paper (see [30]). The mathematical formulation provides a nonlinear approach inspired from a linear theory initially developed by Wagner, von Kármán and Sears [8]. We will provide a brief description for the implementation of these methods and will include some very interesting comparisons between the two methods and further between Wu's method and experiments. Sections 5–7 will show our implementation for these methods on various examples. The modified vortex blob method will be applied for a wing advancing at a given incidence angle. Wu's method will also be applied to solve the same problem, as well as for a wing in heaving, pitching, bending motions and for a wing undergoing highly curved Heaviside and Fourier motions. The two methods will be compared against experiments and we will demonstrate the superiority of Wu's method. Moreover, the lift and thrust will be analyzed in some significant cases and Wagner's result will be numerically implemented using Wu's method. Section 8 is devoted to concluding remarks.

2. Krasny's vortex blob method

2.1. Vortex formation at the edge of a circular tube by a moving piston

Regarding an experiment of Didden in 1979, Krasny and Nitsche [21] implemented a numerical method for the axisymmetric flow shedding a vortex wake. Didden's experiment investigated the movement of a piston inside a circular tube forcing the fluid out and generating a vortex ring at the outer edge of the tube. Comparison between the numerical simulation and experiment shows that the theoretical model captures the basic features of the ring formation process.

The vortex-sheet model has been used extensively to compute flows separating from a sharp edge. The computations employed a time-stepping procedure in which discrete vortex elements of suitable strength were released from the trailing edge advancing at regular time intervals. Instead of using point vortices, Krasny used blobs, meaning that the blobs gave a non-zero radius (δ) to the released vortex elements. This was used to regularize the roll-up of the free vortex sheet (see [2]). The artificial smoothing parameter $\delta > 0$ was used in

the equation governing the motion of the sheet. Krasny used the vortex-sheet model as an approximation to slightly viscous flow. He succeeded in demonstrating the validity of his model by comparing his computational results with some very accurate measurements of a well-controlled experiment for flows past a sharp edge.

2.2. Vortex formation at the edges of a free falling plate

One example considered by Krasny is the movement of a two-dimensional flat plate held normal to the free stream. In this problem, the flow generates two rolled-up vortex sheets, one at each of the two plate edges in symmetry.

A vortex sheet is defined by a curve $z(\Gamma,t)$ in the complex z-plane depending on two parameters: circulation Γ and time t. The evolution equation is

$$\frac{\partial \bar{z}}{\partial t}(\Gamma,t)=\int_C K(z(\widetilde{\Gamma},t)-z(\Gamma,t))\mathrm{d}\widetilde{\Gamma},\quad K(z)=\frac{1}{2\pi \mathrm{i}z}, \tag{1}$$

where $\bar{z}$ is the complex conjugate of the complex space coordinate $z=x+\mathrm{i}y$, the integral assumes its Cauchy principal value, and Γ is the circulation around the vortex sheet lying on an open contour C clockwise (by this convention) from a point below to a point above the point z on the sheet. This is a special case of the Biot–Savart law, which holds only when both points $z(\Gamma,t)$ and $z(\widetilde{\Gamma},t)$ are lying on the contour. It expresses that the mean velocity (averaged across the vortex sheet) on the left-hand side of (1) is equal to the given integral over the vorticity in incompressible flow. (For a proof of this formula and the associated mean velocity, see the derivation below (25) and (26).)

For computational purposes, Chorin's vortex blob method is applied, and the singular kernel in (1) is replaced by the smooth approximation K_δ which approaches our original kernel as δ approaches zero. For example, in free space this becomes

$$K_\delta(z)=K(z)\frac{|z|^2}{|z|^2+\delta^2}. \tag{2}$$

By substituting this regularized kernel into the evolution equation, we obtain a smoothed approximation to the vortex sheet. The curve is discretized into vortex blobs $z_j(t)$ and the integral with the smoothed kernel can be approximated by a trapezoidal rule

$$\frac{\partial \overline{z_j}}{\partial t}=\sum_k K_\delta(z_k-z_j)\Gamma_k. \tag{3}$$

By integrating these equations in time steps we can obtain the motion of the vortex blobs.

Krasny compared his results with that obtained by Pullin in 1978, who used point vortices to represent the vortex sheet, a single point vortex to represent the inner spiral turns, and conformal mappings to determine the strength of the bound vortex sheet. The pair of counter-rotating vortices forming in the recirculating region behind the plate agree very well between the two methods.

Krasny [11] also presented a careful study of the vortex sheet roll-up from a semi-infinite flat plate in his paper. His method can be modified to study forward flying wings, although this was not considered in his papers. To get one step closer to numerically implementing Wu's method, we try to implement this modified method for forward flying wings and compare the results between the modified vortex blob method and Wu's method. The implementation of the modified vortex blob method is based on the theory from the two previous cases and some very useful ideas from Katz and Plotkin [9].

3. Wu's analytical method

As noted in the Introduction, the slender-body theory was developed for expounding fish locomotion by Lighthill [13,14], Wu [29], Newman and Wu [19,20], Newman [18] and others. This theory is applicable to a very general class of body geometry and movement, from the propulsive motions in carangiform and thunniform to those in amiiform and gymnotiform. In all the cases the body may be regarded as slender,

characterized by a small slenderness parameter, δ, defined as the ratio of maximum body depth to body length, $\delta = 2b/l$. The theory is based on the assumption that the amplitude of the undulatory wave motion passed along the body is small compared to body length, so that its higher nonlinear effects can be neglected. The Reynolds number, for the cases of practical interest, is usually high, ranging over 10^4–10^7. Newman and Wu showed in 1972 that the effect of body thickness in the direction of bodily displacement (in the z-direction) from the stretched-straight position (in the xy-plane) is secondary in effect and can be neglected. Later on, Newman [18] and Newman and Wu [20] showed this effect could be retrieved if desired by employing conformal mapping to map cross-sectional body contour into a slit so as to make use of the solution to zero-thickness case.

3.1. The nonlinear theory of 2D flexible lifting-surface locomotion

3.1.1. Problem setup

The theory of two-dimensional lifting-surface locomotion is very important, both because it provides a very good limiting case for asymptotic evaluation of lifting-surfaces of large aspect-ratio as found in many cases of aquatic and aerial animal locomotion, and because it provides a very good starting point for the development of a three-dimensional generalized theory.

We consider the irrotational flow of an incompressible and inviscid fluid generated by a thin two-dimensional surface S_b (of zero thickness), performing an arbitrary motion through the fluid, and simulating with its flexibility the movement of animals in nature. We then parameterize this motion by using a Lagrangian coordinate ξ to express a point $(X(\xi,t), Y(\xi,t))$ on S_b varying in time as

$$S_b(t) : \mathbf{x} = \mathbf{X}(\xi,t) = (X(\xi,t), Y(\xi,t)) \quad (-1 < \xi < 1, t \geqslant 0). \tag{4}$$

The simplest choice of ξ is the initial material position of $S_b(t=0)$ which is taken to be in its stretched-straight shape so that $X(\xi,0) = \xi, Y(\xi,0) = 0 (-1 < \xi < 1)$, lying in an unbounded fluid initially at rest in an inertial frame of reference (see Fig. 1). The body surface $S_b(t)$ can be flexible but is considered inextensible, so that

$$X_\xi^2 + Y_\xi^2 = 1. \tag{5}$$

The moving surface $S_b(t)$ has its tangential $\mathbf{s}$ and normal $\mathbf{n}$ unit vectors given by

$$\mathbf{s}(\xi,t) = \partial\mathbf{X}/\partial\xi = (X_\xi, Y_\xi), \quad \mathbf{n}(\xi,t) = (-Y_\xi, X_\xi). \tag{6}$$

The velocity of a point designated by ξ on $S_b(t)$ is prescribed by

$$\mathbf{U}(\xi,t) = \partial\mathbf{x}/\partial t = (X_t, Y_t), \quad (-1 < \xi < 1, t \geqslant 0) \tag{7}$$

and its tangential and normal components are found by projecting the velocity accordingly as

$$U_s(\xi,t) = \mathbf{U}\cdot\mathbf{s} = (X_\xi X_t + Y_\xi Y_t), \quad U_n(\xi,t) = \mathbf{U}\cdot\mathbf{n} = (X_\xi Y_t - Y_\xi X_t). \tag{8}$$

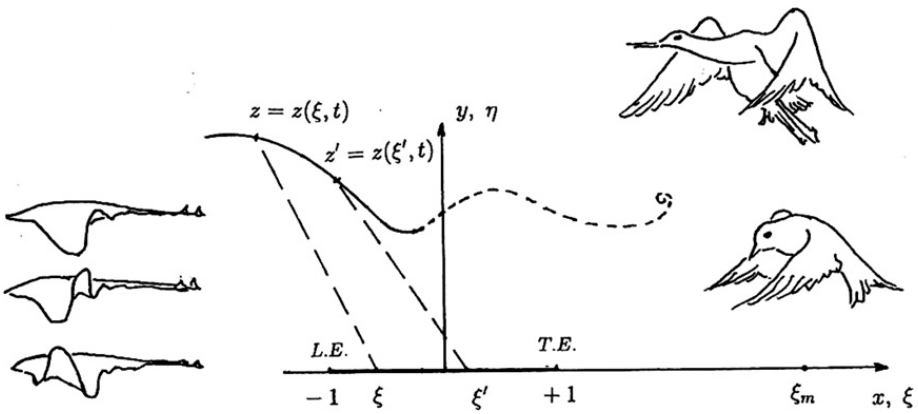

Fig. 1. The Lagrangian coordinate system, (ξ,η), used to describe arbitrary motion of a two-dimensional flexible lifting-surface moving along arbitrary trajectory through an incompressible and inviscid fluid in a reference frame (x,y) fixed with the fluid at infinity.

As stated before, the flow field is expressed in Eulerian coordinates, so the velocity of the incompressible and irrotational flow has a velocity potential $\phi(x,y,t)$ and a stream function $\psi(x,y,t)$. The complex coordinate z, complex potential f and complex velocity w are given by

$$z = x + \mathrm{i}y, \quad f = \phi + \mathrm{i}\psi, \quad w = u - \mathrm{i}v = \mathrm{d}f/\mathrm{d}z \tag{9}$$

and they are analytic functions of one another.

3.1.2. Boundary conditions

Next we express all the boundary conditions in terms of these variables. We will adopt a set of coordinates (ξ,η), with the η-axis pointing in the direction of the normal vector $\mathbf{n}$, where $\eta = 0$ coincides with $S_b(t)$ for $(-1 < \xi < 1, t \geqslant 0)$. After the motion starts, a free vortex sheet is shed from the trailing edge (TE at $\xi = 1$) to form a wake surface $S_w(t)$ described by the extended material coordinate ξ for $\xi > 1$

$$S_w(t) : \mathbf{x} = \mathbf{X}(\xi,t) = (X(\xi,t), Y(\xi,t)), \quad (1 < \xi < \xi_m, t \geqslant 0), \tag{10}$$

where ξ_m identifies the trajectory $(X(\xi_m,t), Y(\xi_m,t))$ of the very first (starting) vortex filament released into the wake. Hence, at each and every time step a new stretch is being created in the wake just beyond the trailing edge, $\delta\mathbf{X}(1,t) = \mathbf{U}(1,t)\delta t$, tangentially to the trajectory of the trailing edge which is advancing with velocity $\mathbf{U}(1,t)$, which can be modified at a higher order by the mean velocity of the fluid leaving the trailing edge.

Using analytic continuation, we can think of (ξ,η) as forming a complex reference plane $\zeta = \xi + \mathrm{i}\eta$ so that the two planes, ζ and $z = x + \mathrm{i}y$ are related by a conformal transformation which will be denoted by $z = z(\zeta,t)$. There is no need to determine the actual conformal mapping $z = z(\zeta,t)$ since we only have to use its analytic relationship in a small neighborhood of $S_b(t) + S_w(t)$.

Now we introduce a transformation between the Eulerian coordinates (x,y,t) and the Lagrangian material ones $(\xi,\eta,t\prime)$

$$x = \tilde{x}(\xi,\eta,t'), \quad y = \tilde{y}(\xi,\eta,t'), \quad t = t', \quad F(x(\xi,\eta,t'),y(\xi,\eta,t'),t) = \widetilde{F}(\xi,\eta,t'), \tag{11}$$

where F being any differentiable function. By the chain rule, for this kind of general function we have

$$\frac{\partial\widetilde{F}}{\partial t'} = \left.\frac{\partial\widetilde{F}}{\partial t'}\right|_{\xi,\eta} = \frac{\partial F}{\partial t} + u\frac{\partial F}{\partial x} + v\frac{\partial F}{\partial y} \equiv \frac{\mathrm{d}F}{\mathrm{d}t}, \tag{12}$$

which is the material time derivative by following the fluid particle designated by (ξ,η) at time instant $t' = t$. Using these relations we will derive some useful properties for the quantities of interest. For a general flow variable, we denote its value on the $\pm$ side of S_b or S_w by

$$\widetilde{F}(\xi,\eta = \pm 0,t') = \widetilde{F}_{\pm}(\xi,t'), \quad (-1 < \xi < \xi_m, t \geqslant 0). \tag{13}$$

The variables with subindices $\pm$ are called surface variables and they are computed for the upper and lower boundaries of the surface. Their derivatives are given by (12),

$$\frac{\partial\widetilde{F}_{\pm}}{\partial t'} = \left(\frac{\mathrm{d}F}{\mathrm{d}t}\right)_{\pm} = \left(\frac{\partial F}{\partial t}\right)_{\pm} + \mathbf{u}_{\pm}\cdot(\nabla F)_{\pm}, \quad (\mathbf{u}_{\pm} = (u_{\pm}, v_{\pm}), \quad \nabla = (\partial_x, \partial_y)), \tag{14}$$

and

$$\frac{\partial\widetilde{F}_{\pm}}{\partial\xi} = \mathbf{s}\cdot(\nabla F)_{\pm}, \quad \left(\frac{\partial\widetilde{F}}{\partial\eta}\right)_{\pm} = \mathbf{n}\cdot(\nabla F)_{\pm}, \tag{15}$$

where the operator $\partial_{t'}$ means the material time-rate of change, the operator ∂_ξ gives the surface gradient and ∂_η the normal gradient.

To compute the velocities of the particles along both sides of $S_b \cup S_w$ at $\mathbf{X}(\xi,t)$, we have

$$\mathbf{u}_{\pm}(\xi,t') = \partial\mathbf{x}_{\pm}(\xi,t')/\partial t', \quad (-1 < \xi < \xi_m, t' > 0), \tag{16}$$

which in complex form becomes

$$\frac{\partial z_{\pm}}{\partial t'}(\xi,t') = \bar{w}_{\pm}(\xi,t'), \tag{17}$$

where the over-line means complex conjugate. Decomposing the velocity into tangential and normal components, we have, in complex form,

$$u_s^{\pm} - \mathrm{i}u_n^{\pm} = (u_{\pm} - \mathrm{i}v_{\pm})(X_{\xi} + \mathrm{i}Y_{\xi}) = w_{\pm}(\xi,t')\frac{\partial Z(\xi,t')}{\partial \xi}, \quad (Z = X + \mathrm{i}Y). \tag{18}$$

The kinematic condition requires that any fluid particle that is situated on the boundary surface at some time will for ever remain on it. This can be written as

$$u_n^{+}(\xi,t') = u_n^{-}(\xi,t') = U_n(\xi,t') \quad \text{on} \quad S_b(t) \cup S_w(t), \quad (-1 < \xi < \xi_m, t' > 0). \tag{19}$$

This means of course that there is no flow through the surface. Tangential to the surface the condition is different since the tangential velocity at the boundary surface develops a jump in magnitude across the surface. Hence, $S_b(t)$ becomes a bound vortex sheet while $S_w(t)$ is a free vortex sheet which is convected away with the fluid. The above relations say that $U_n(\xi,t')$ is prescribed on $S_b(t)$ but is unknown on $S_w(t)$, which requires to be calculated by imposing a dynamic condition on $S_w(t)$, namely that the pressure must be continuous on $S_w(t)$

$$p_{+}(\xi,t') = p_{-}(\xi,t'), \quad (1 \leqslant \xi < \xi_m, t > 0), \tag{20}$$

which invokes no pressure jump across the free sheet, including the trailing edge at $\xi = 1$, which is the Kutta condition. The pressure is given by the Bernoulli equation

$$\frac{p}{\rho} + \frac{\partial \phi}{\partial t} + \frac{1}{2}(u_s^2 + u_n^2) = \frac{p}{\rho} + \frac{\partial \phi}{\partial t'} - \frac{1}{2}(u_s^2 + u_n^2) = 0, \tag{21}$$

where the latter one follows from using (12). Furthermore, using condition (19) we get

$$\frac{1}{\rho}(p_- p_+) = \left(\frac{\partial \phi}{\partial t}\right)_+ - \left(\frac{\partial \phi}{\partial t}\right)_- + \frac{1}{2}(u_s^+ + u_s^-)(u_s^+ - u_s^-) = \frac{\partial}{\partial t'}(\phi_+ - \phi_-) - \frac{1}{2}(u_s^+ + u_s^-)(u_s^+ - u_s^-), \quad (z \in S_b \cup S_w).$$

3.1.3. Integral equation formulation

To find the unique solution to our problem, we follow the approach from (1) and adopt the integral representation of the complex velocity $w = u - \mathrm{i}v = \mathrm{d}f/\mathrm{d}z$ in terms of a surface distribution of vorticity of strength $\gamma(\xi',t)$ over the boundary surface, which gives

$$w(z,t) = \frac{1}{2\pi \mathrm{i}} \int_{S_b \cup S_w} \frac{\gamma(\xi',t)}{z' - z}\,\mathrm{d}\xi', \quad (\gamma = u_s^+ - u_s^- = \partial \Gamma/\partial \xi, z \notin S_b \cup S_w). \tag{22}$$

By applying Plemelj's formula to (22) we obtain

$$w_{\pm}(z,t) = \pm\frac{1}{2}\gamma(\xi,t)/\frac{\mathrm{d}z}{\mathrm{d}\xi} + \frac{1}{2\pi \mathrm{i}} \int_{S_b \cup S_w} \frac{\gamma(\xi',t)}{z' - z}\,\mathrm{d}\xi', \quad (z = Z(\xi,t) \in S_b \cup S_w), \tag{23}$$

in which the integral assumes its Cauchy principal value as understood. Now from (23) and (18),

$$u_s^{\pm} - \mathrm{i}u_n^{\pm} = \pm\frac{1}{2}\gamma(\xi,t) + \frac{1}{2\pi \mathrm{i}}\frac{\mathrm{d}z}{\mathrm{d}\xi} \int_{S_b \cup S_w} \frac{\gamma(\xi',t)}{z' - z}\,\mathrm{d}\xi'. \tag{24}$$

Of course, this result validates (19) and gives

$$u_n^{+}(\xi,t) = u_n^{-}(\xi,t) = \frac{1}{2\pi}\Re\left\{\frac{\mathrm{d}z}{\mathrm{d}\xi} \int_{S_b + S_w} \frac{\gamma(\xi',t)}{z' - z}\,\mathrm{d}\xi'\right\}, \tag{25}$$

$$u_{sm} \equiv \frac{1}{2}(u_s^+ + u_s^-) = \frac{1}{2\pi}\Im\left\{\frac{\mathrm{d}z}{\mathrm{d}\xi} \int_{S_b + S_w} \frac{\gamma(\xi',t)}{z' - z}\,\mathrm{d}\xi'\right\}, \tag{26}$$

where $\Re$ and $\Im$ stand for the real and imaginary part of what follows. In passing, we note that combining (25) and (26) under (18) yields (1) as a proof, noting that $\gamma = \partial \Gamma/\partial \xi$. These equations will play a very important

role in the implementation of the numerical method. The first one shows the continuity of the normal velocity across the vortex sheet, while the second one gives an average of the tangential component of the velocity across the boundary $S_b \cup S_w$. These relations again give an interpretation of the boundary conditions

on S_b: $u_n(\xi,t) = U_n(\xi,t)$ is prescribed whilst the vorticity $\gamma(\xi,t) = \gamma_b(\xi,t)$ is unknown;
on S_w: $\gamma(\xi,t) = \gamma_w(\xi,t)$ is material invariant, but $u_n(\xi,t)$ and $u_{sm}(\xi,t)$ are unknown.

Here, this material invariance of the vorticity follows from Helmholtz's theorem, which states that in an irrotational flow of an incompressible inviscid fluid, vorticity cannot be generated in any interior bulk of the fluid but can only at a boundary surface. Once it is generated at a surface, it will be conserved in time after leaving the surface. Hence, invoking this vorticity conservation law on the vorticity after being shed with the local fluid, we have

$$\frac{\partial \gamma_w}{\partial t} + u_{sm}\frac{\partial \gamma_w}{\partial \xi} = 0, \quad (1 \leqslant \xi < \xi_m, t > 0). \tag{27}$$

Its continuous integral at the trailing edge ($\xi = 1$) can serve as the Kutta condition like (20). This will help compute the trajectory of the free vortex sheet by a time-marching procedure.

3.1.4. Additional equation

One more condition concerning the total circulation which is needed for the solution comes from Kelvin's circulation theorem stating that the total circulation is conserved in time. The circulation $\Gamma(\xi,t)$ can be expressed as the integral of vorticity distribution as

$$\Gamma(\xi,t) = \oint_{P_-}^{P_+} \mathbf{u}\cdot \mathrm{d}\mathbf{x} = \int_0^{\xi} (u_s^+ - u_s^-)\mathrm{d}\xi = \int_0^{\xi} \gamma(\xi,t)\mathrm{d}\xi, \quad (-1 < \xi < \xi_m, t > 0), \tag{28}$$

where the contour is just that defined for Γ in (1). Hence, by Kelvin's theorem, the total circulation around any closed contour Σ encircling completely the entire vortex sheet remains fixed in time,

$$\Gamma_\Sigma(t) = \int_0^{\xi_m} \gamma(\xi,t)\mathrm{d}\xi = \Gamma(0), \quad (t \geqslant 0). \tag{29}$$

If the flow starts from rest, $\Gamma(0) = 0$. It is of particular interest to split the integral in (29) into two parts to have the circulations about the bound and the free vortex sheets related by

$$\Gamma_b(t) = \oint_{S_b} \mathbf{u}\cdot \mathrm{d}\mathbf{x} = \int_0^1 \gamma(\xi,t)\mathrm{d}\xi = -\int_1^{\xi_m} \gamma(\xi,t)\mathrm{d}\xi = -\Gamma_w(t). \tag{30}$$

We use this expression because, eventually, we are interested in the circulation of the newly released vortex filament. To be able to compute this circulation we consider the variation $\delta\Gamma_b = \Gamma_b(t+\delta t) - \Gamma_b(t)$ in the bound vortex for a very small time interval δt. According to Kelvin's theorem, the variation of $\Gamma_b(t)$ is equal to that of $-\Gamma_w(t)$ in this time interval, or

$$\delta\Gamma_b(t) = -\delta\Gamma_w(t) = -\gamma(1,t)\delta\xi = -\gamma(1,t)[U_s(1,t) + u_{sm}(1,t)]\delta t, \tag{31}$$

where $U_s(1,t)$ is the (given) tangential velocity of the trailing edge. The circulation of the previously shed free vortex sheet does not appear in this relation, since it remains conserved in time.

The theory presented above is sufficient to produce a time-marching numerical procedure described by Wu ([30]). However, Wu took the theory even further and after some more theoretical results, he proposed a new numerical method based on the time-marching procedure and on the extended theory. Here, we will first present the theoretical results from this paper and then describe the complete numerical recipe.

3.2. Generalized Wagner–von Kármán–Sears method – Wu's method

As mentioned in the Introduction, there have been several contributions of renown to the advances in linear theory on airfoil in non-uniform motion. The one of especial interest toward readily affording generalizations

for nonlinear considerations is that by von Kármán and Sears [8]. Their theory has further advanced the pioneering work of Wagner [28] who derived an integral equation to calculate the wake vorticity shed from a wing. In an improved way, von Kármán and Sears developed a very ingenious decomposition of the bound vorticity distribution γ_b into two parts, one for the "quasi-stationary, wake-less" flow, γ_0, and the other, γ_1, due to the effect of the trailing vortex sheet on the wing. The uniqueness and importance of this method therefore provides a direct generalization to a fully nonlinear theory. Theodore Wu [30] improved this idea even further, generalizing it to two-dimensional flexible lifting surface performing arbitrary motion for modeling aquatic and aerial animal locomotion.

3.2.1. Vorticity distribution

Following von Kármán and Sears, we have the vorticity $\gamma_b(\xi,t)$ bound to S_b split into two parts and distributed with the free vorticity $\gamma_w(\xi,t)$ in the wake as follows:

$$\begin{aligned}&\text{on } S_b(t): \gamma(\xi,t)=\gamma_b(\xi,t)=\gamma_0(\xi,t)+\gamma_1(\xi,t), \quad (-1<\xi<1, t\geqslant 0),\\ &\text{on } S_w(t): \gamma(\xi,t)=\gamma_w(\xi,t), \quad (1<\xi<\xi_m, t\geqslant 0),\end{aligned}$$

where $\gamma_0(\xi,t)$ is the "quasi-stationary, wake-less" vorticity mentioned above, and $\gamma_1(\xi,t)$ is the additional bound vorticity required to cancel the effect due to the trailing wake vortices $\gamma_w(\xi,t)$ on the normal velocity at the wing. To determine these vortex distributions we will follow the next three steps:

(1) determine $\gamma_0(\xi,t)$ using the prescribed $U_n(\xi,t)$ with t fixed and no unsteady wake;
(2) determine $\gamma_1(\xi,t)$ due to the effect of wake vortex γ_w so as to reinstate the unsteady $U_n(\xi,t)$;
(3) determine $\gamma_w(\xi,t)$ at $\xi=1$ under the Kutta condition and for $1<\xi<\xi_m$ by integrating (27).

We should emphasize that this approach will take into account the nonlinear effects given by the actual displacement of the vortex sheet, which makes this theory significantly different from the linear one. The three steps necessary for finding the vorticity both on the wing and in the wake will be described below in more detail.

Step 1. To compute $\gamma_0(\xi,t)$ we omit the wake effect and regard the time as a fixed parameter. Thus, by (19) and (25)

$$U_n(\xi,t)=\frac{1}{2\pi}\Re\left\{\frac{\mathrm{d}z}{\mathrm{d}\xi}\int_{-1}^{1}\frac{\gamma_0(\xi',t)}{z(\xi',t)-z(\xi,t)}\,\mathrm{d}\xi'\right\}, \quad (-1<\xi<1), \tag{32}$$

which basically is a singular integral equation that will give us $\gamma_0(\xi,t)$ under the Kutta condition. To see this, we rewrite (32) to single out the Cauchy kernel,

$$\begin{aligned}U_n(\xi,t)&=\frac{1}{2\pi}\int_{-1}^{1}\left[\frac{1}{\xi'-\xi}+g(\xi',\xi)\right]\gamma_0(\xi',t)\mathrm{d}\xi'\equiv(G_0+G_1)\gamma_0,\\ g(\xi',\xi)&=\Re\left\{\frac{z_\xi(\xi,t)}{z(\xi',t)-z(\xi,t)}\right\}-\frac{1}{\xi'-\xi},\end{aligned} \tag{33}$$

where $(\xi'-\xi)^{-1}$ is the Cauchy kernel while $g(\xi',\xi)$ is a smooth kernel. Note that for a flat-plate airfoil, both z and z' will be on the wing, making $\mathrm{d}z/\mathrm{d}\xi$ a constant, and therefore making $g(\xi',\xi)=0$, which is the linear case as expected. For slightly curved body movement, $|g(\xi',\xi)|$ is small, so we can solve (32) by iteration with $\gamma_0(\xi,t)$ expanded in terms of the small bound of $|g(\xi',\xi)|$ as

$$\gamma_0=\gamma_{00}+\gamma_{01}+\gamma_{02}+\cdots. \tag{34}$$

Substituting (34) in (33) and matching terms of the same order, we attain

$$G_0\gamma_{00}=\frac{1}{2\pi}\int_{-1}^{1}\frac{1}{\xi'-\xi}\gamma_{00}(\xi',t)\mathrm{d}\xi'=U_n(\xi,t), \quad (-1<\xi<1), \tag{35}$$

$$G_0\gamma_{0k}=\frac{1}{2\pi}\int_{-1}^{1}\frac{1}{\xi'-\xi}\gamma_{0,k-1}(\xi',t)\mathrm{d}\xi'\equiv -G_1\gamma_{0,k-1}, \quad (k=1,2,\ldots). \tag{36}$$

The leading order equation (35) can be solved in closed form under the Kutta condition, giving

$$\gamma_{00}(\xi,t) = -\frac{2}{\pi}\sqrt{\frac{1-\xi}{1+\xi}}\int_{-1}^{1}\sqrt{\frac{1+\xi'}{1-\xi'}}\frac{U_n(\xi',t)}{\xi'-\xi}\,\mathrm{d}\xi' \equiv G_0^{-1}U_n, \quad (-1<\xi<1). \tag{37}$$

This can be easily verified by substituting (37) in (35) and using the Poincaré–Bertrand formula (see [17, Section 23, Eq. (23.7)])

$$\int_L \frac{\mathrm{d}\xi'}{\xi'-\xi}\int_L \frac{h(\xi',\xi'')}{\xi''-\xi'}\,\mathrm{d}\xi'' = -\pi^2 h(\xi,\xi) + \int_L \mathrm{d}\xi''\int_L \frac{h(\xi',\xi'')}{(\xi'-\xi)(\xi''-\xi')}\,\mathrm{d}\xi'. \tag{38}$$

Putting everything together, we find all the terms in the expansion (34) summed up for $\gamma_0(\xi,t)$ as

$$\gamma_0(\xi,t) = G_0^{-1}(U_n+N_0), \quad N_0 = \sum_{m=1}^{N}(-1)^m(G_1G_0^{-1})^m U_n \equiv G_N U_n, \quad (N<\infty). \tag{39}$$

Thus, given U_n (the body motion) by (8), we have found the vorticity γ_0 which also gives the corresponding circulation as

$$\Gamma_0(t) = \int_{-1}^{1}\gamma_0(\xi,t)\,\mathrm{d}\xi = -2\int_{-1}^{1}\sqrt{\frac{1+\xi}{1-\xi}}[U_n(\xi,t)+N_0(\xi,t)]\mathrm{d}\xi. \tag{40}$$

This ends step 1. In step 2, we proceed to find γ_1 due to the effect of $\gamma_w(\xi,t)$ $(1<\xi\leqslant\xi_m)$ to reinstate the prescribed unsteady $U_n(\xi,t)$ on the plate, first for γ_w at the trailing edge, $\xi=1$, and then for $1<\xi\leqslant\xi_m$ by integrating (27), thus resolving γ_1 in terms of a functional of γ_w.

Step 2. First, from (25) we have the expression for the normal velocity $U_{n1}(\xi,t)$ induced at $z(\xi,t)$ on S_b by the free vortex sheet γ_w given in terms of the integral operator $K = K_0 + K_1$ as

$$U_{n1}(\xi,t) = \frac{1}{2\pi}\Re\left\{\frac{\mathrm{d}z}{\mathrm{d}\xi}\int_1^{\xi_m}\frac{\gamma_w(\xi',t)}{z'-z}\mathrm{d}\xi'\right\} \equiv (K_0+K_1)\gamma_w, \quad (-1<\xi<1), \tag{41}$$

$$K_0\gamma_w = \frac{1}{2\pi}\int_1^{\xi_m}\frac{\gamma_w(\xi',t)}{\xi'-\xi}\mathrm{d}\xi', \quad K_1\gamma_w = \frac{1}{2\pi}\int_1^{\xi_m} g(\xi',\xi)\gamma_w(\xi',t)\mathrm{d}\xi', \tag{42}$$

where $g(\xi',\xi)$ is the same as that defined in step 1 except that in this case the ranges for ξ' and ξ are $1<\xi'<\xi_m$ and $-1<\xi<1$. Here, U_{n1} is the normal velocity on the wing S_b induced by wake vortex γ_w (yet unknown). Then a bound vorticity γ_1 is required to satisfy (32) but with U_n replaced by $-U_{n1}$ so that the unsteady $U_n(\xi,t)$ is restored. Hence exactly similar to (39) we obtain

$$\gamma_1(\xi,t) = -G_0^{-1}[U_{n1}+N_1], \quad N_1 = \sum_{m=1}^{N}(-1)^m(G_1G_0^{-1})^m U_{n1} = G_N U_{n1}, \quad (N<\infty). \tag{43}$$

Substituting (41) in (43) and performing some algebra, we find

$$\gamma_1(\xi,t) = \gamma_{10}(\xi,t)+\gamma_{1N}(\xi,t), \quad \gamma_{10} = -G_0^{-1}K_0\gamma_w, \quad \gamma_{1N} = -G_0^{-1}G_N U_{n1}, \tag{44}$$

$$\gamma_{10} = \frac{1}{\pi}\sqrt{\frac{1-\xi}{1+\xi}}\int_1^{\xi_m}\sqrt{\frac{\xi'+1}{\xi'-1}}\frac{\gamma_w(\xi',t)}{\xi'-\xi}\,\mathrm{d}\xi', \quad (-1<\xi<1), \tag{45}$$

$$\gamma_{1N} = \frac{1}{\pi^2}\sqrt{\frac{1-\xi}{1+\xi}}\int_1^{\xi_m}\gamma_w(\xi',t)\mathrm{d}\xi'\int_{-1}^{1}\sqrt{\frac{1+\xi''}{1-\xi''}}\frac{g(\xi',\xi'')+G_N K(\xi',\xi'')}{\xi''-\xi}\mathrm{d}\xi'', \tag{46}$$

where (45) comes by interchanging the order of integrations. Thus, γ_1 is expressed in terms of γ_w.

Step 3. This bound vorticity γ_1 then generates an additional circulation Γ_1 around the wing,

$$\Gamma_1(t) = \int_{-1}^{1} \gamma_1(\xi, t)\mathrm{d}\xi = \Gamma_{10}(t) + \Gamma_{1N}(t), \tag{47}$$

$$\Gamma_{10} = \int_{-1}^{1} \gamma_{10}(\xi, t)\mathrm{d}\xi = \int_{1}^{\xi_m} \left(\sqrt{\frac{\xi+1}{\xi-1}} - 1\right)\gamma_w(\xi, t)\mathrm{d}\xi, \tag{48}$$

$$\Gamma_{1N} = \frac{1}{\pi}\int_{1}^{\xi_m} \gamma_w(\xi, t)\mathrm{d}\xi \int_{-1}^{1} \sqrt{\frac{1+\xi'}{1-\xi'}}[g(\xi, \xi') + G_N K(\xi, \xi')]\mathrm{d}\xi'. \tag{49}$$

Now, the total circulation around the wing S_b is of course $\Gamma_b = \Gamma_0 + \Gamma_1$ while the total circulation around the free vortex sheet Γ_w is given by

$$\Gamma_w(t) = \int_{1}^{\xi_m} \gamma_w(\xi, t)\mathrm{d}\xi. \tag{50}$$

Finally, applying Kelvin's theorem to invoke that the total circulation around the wing and the wake be conserved yields

$$\Gamma_b + \Gamma_w = \Gamma_0 + \Gamma_1 + \Gamma_w = 0, \tag{51}$$

which gives

$$\Gamma_0 + \int_{1}^{\xi_m} \sqrt{\frac{\xi+1}{\xi-1}}\gamma_w(\xi, t)\mathrm{d}\xi + \Gamma_{1N} = 0. \tag{52}$$

This is the generalized nonlinear Wagner's integral equation for the trailing vortex distribution γ_w. In this last equation, Γ_{1N} and N_0 in Γ_0 of (40) represent all the nonlinear effects. If we disregard these two terms the original Wagner's linear equation is recovered.

3.2.2. The numerical algorithm

To discretize all the equations above to be used in our numerical method, we choose a time sequence $t_0 = 0, t_1, t_2, \ldots, (t_k - t_{k-1} = \Delta t_k, k = 1, 2, \ldots)$, with sufficiently small Δt_k. At time t_0 the body is found in the stretched-straight position in the unbounded flow which is at rest. After Δt_1, i.e. at time t_1, the bound sheet $S_b(t_1)$ has just arrived at a new position according to (4), thus opening up behind the trailing edge a free filament $\Delta\xi_1$ as the very first onset grid in the wake S_w (see 31) to receive the starting vortex element just shed. The unknown vorticity $\gamma_b(\xi, t)$ on the wing is determined separately for its two components $\gamma_0(\xi, t)$ and $\gamma_1(\xi, t)$, $\gamma_0(\xi, t)$ being first determined by (39). To determine $\gamma_1(\xi, t)$, we first solve for $\gamma_w(\xi, t)$ by (52) and then for $\gamma_1(\xi, t)$ using (44)–(46). In this way, the total vorticity on the wing, $\gamma_b(\xi, t) = \gamma_0(\xi, t) + \gamma_1(\xi, t)$, as well as the vorticity of the newly released wake element $\gamma_w(\xi, t_1)$, are all determined. Thus, we know the vorticity along the whole sheet $(1 < \xi < 1 + \Delta\xi_1)$, and we can determine u_{sm} by (26) and u_n by (25) on $\Delta\xi_1$ of $S_w(t_1)$. Then we can revise the data on the length and direction of $\Delta\xi_1$ in $S_w(t_1)$ by iteration for any improvement.

At t_2, the wing has moved again according to (4) to its new position $\mathbf{X}(\xi, t_2)$. The vortex released at the previous time t_1 has been convected downstream at the flow velocity, with its circulation preserved in magnitude with time. The movement of the wing opens again a new onset grid in the wake, allowing receipt of a new free vortex element in the wake over the stretch $\Delta\xi_2$. We can again go through all the same calculations as performed at the previous time step, i.e., compute the vorticity of the whole vortex sheet, the normal and tangential velocities and eventually updating the data on S_w. Thus, we have just constructed an algorithm that will take us from any known time step at t_k to the next one at t_{k+1}. It is therefore clear that an incredibly important role played in the determination of the vorticity is at each currently shedding of a new free vortex element. The in-depth numerical procedure for discretizing the equations given above will be presented in the following section.

4. Numerical implementation of the modified vortex blob method

4.1. Vortex forming behind a wing advancing at a given angle of attack

Our implementation of the modified vortex blob method for a wing advancing at a given angle of attack is based on the evolution equation (1). The idea presented in the previous two sections will work here too, since

by discretizing this evolution equation we get a linear system that will give us the circulation on the wing. The discretization of the equation shows that if a vortex element of circulation Γ is located at (x_0, y_0), then the velocity induced by this element at an arbitrary point $P(x, y)$ will be

$$u(x,y) = \frac{\Gamma}{2\pi} \frac{(y - y_0)}{(x - x_0)^2 + (y - y_0)^2} \tag{53}$$

$$v(x,y) = \frac{-\Gamma}{2\pi} \frac{(x - x_0)}{(x - x_0)^2 + (y - y_0)^2}. \tag{54}$$

Consider the wing being consisted of a set of bound point vortices distributed by a cosine-distribution ($y = \cos\theta, y_0 = \cos\theta_0$) to achieve a better resolution with more vortices near the trailing and leading edges. Following an idea of Katz ([9]), known as Weissinger's rule in wing theory, the vortices will be placed at the quarter-chord point of each segment, while the normal velocity u_n (known or not) will be collocated at the three-quarter-chord point of each segment, and thereby the Kutta condition will be satisfied automatically (see Fig. 2). Therefore, the boundary condition (no flow through the wing) will be imposed at the collocation points and the circulation will be determined at the location of the vortices. Thus, Eqs. (53) and (54) will not have singularities even when both points are on the wing. However, when the points both lie in the wake, a blob will be used, meaning that we will add a small δ^2 to the denominators of (53) and (54). Suppose we take N points on the wing (in our calculations $N = 40$). Then we will have $N - 1$ vortex points and $N - 1$ collocation points. If at a certain time step we have N_w vortex filaments in the wake, then the velocity of each bound vortex point of the wing is a sum of the velocities induced by the $N - 1$ bound vortices and N_w free vortices. These induced velocities are computed using (53) and (54). The strength of all the wake vortices except the one shed at the current time step is known from the previous time step since it is conserved in time. Therefore, the unknowns here are the values of the circulation of bound vortices ($N - 1$ unknowns) and also the strength of the latest wake vortex. Thus, we have N unknowns and only $N - 1$ equations, i.e. imposing the boundary condition at every collocation point. The Nth linear equation will be given by the Kelvin condition which states that the total circulation is conserved. This means that the sum of the total bound and free circulation is zero if we start from a rest state. So our system will be of the form

$$a_{i1}\Gamma_1 + a_{i2}\Gamma_2 + a_{i3}\Gamma_3 + \cdots + a_{i,N-1}\Gamma_{N-1} + a_{iw}\Gamma_{1w} = b_i \quad i = 1, \ldots, (n-1)$$

$$\Gamma_1 + \Gamma_2 + \Gamma_3 + \cdots + \Gamma_{N-1} + \Gamma_{1w} = b_0 = -\sum_{k>1} \Gamma_{kw},$$

where the right-hand-side terms are the ones known, corresponding to the known wake strengths.

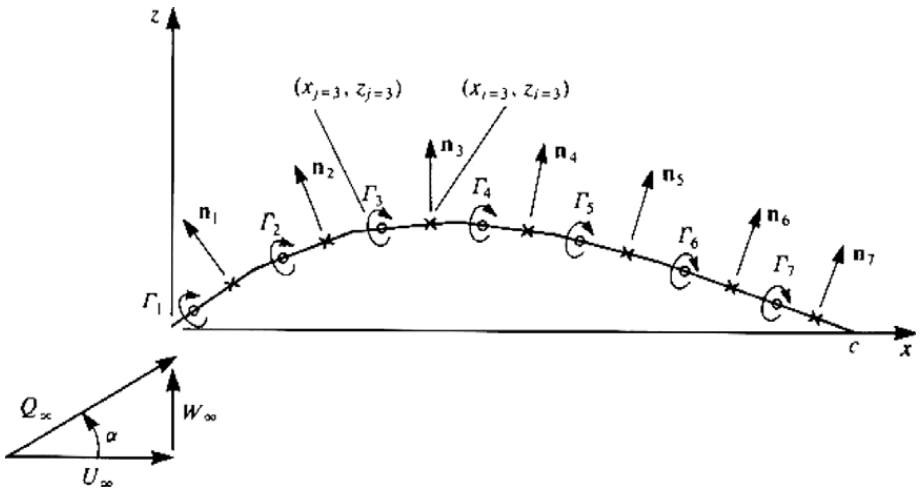

Fig. 2. Discrete vortex representation of the thin, lifting airfoil model.

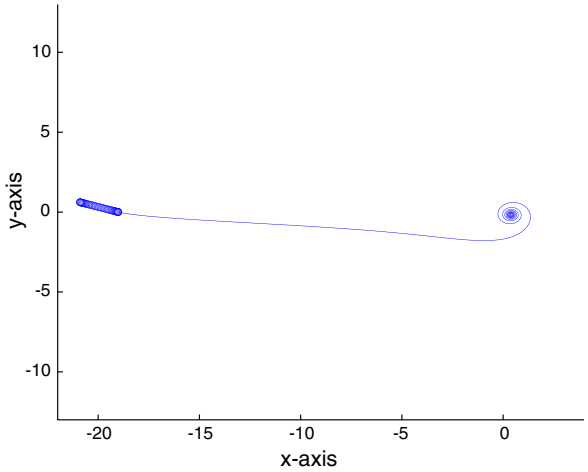

Fig. 3. Modified vortex blob method for a wing advancing with an angle of attack $\alpha = 18^\circ$, with speed $U_0 = 10$, blob $\delta = 0.2$, time-step $dt = 0.0002$. Plot after 10,000 time steps having $N = 40$ bound vortex points.

Remark. The location of the currently released filament is also known, this being placed in the center of the path covered by the trailing edge at the current time step.

In this manner, we are able to solve for the strengths of the bound vortices and the latest released wake filament by solving the linear system. Going back to Eqs. (53) and (54) we can now compute the velocities of all the free vortices and move them accordingly. Please note that there are differences between Krasny's approach and this modified method mainly in the way we compute the characteristics of the newly released vortex element. This ends one time step in our computation. To start the next one, we will move the wing with the prescribed velocity and compute all the above quantities repeatedly.

This result will be compared latter in this section with the one obtained by Wu's method but for now it can be well expected to have all the main features in clear display as desired. For instance, we get more and more roll-ups as we decrease the blob and the interior of the vortex has a very good resolution. For our computations we choose variable time steps, apply insertion techniques both with respect to the distance between the free vortices and to the angular separation and all work fine. The plot in Fig. 3 is obtained with a speed $U_0 = 10$, inclination angle $\alpha = 18^\circ$ and blob $\delta = 0.2$, the chord-length being $c = 2$. The time step is chosen relatively small $dt = 0.0002$ since we leave our method to run for 10,000 time-steps. This corresponds to the wing covering a distance equal to 10 chord lengths. We can see that even after such a long computation, the method is very robust giving a very nice roll-up. We note that throughout our simulations we preferred to use a constant time-step since we could not get any significant improvement from some complicated time-stepping procedures.

At this point, knowing all these tricks about vortex theory, we are ready to attack Wu's method. Even more, we now have some very important results for comparison with other methods.

5. Numerical implementation of Wu's method

5.1. Vortex forming behind a wing advancing at a given angle of attack modeled by Wu's method

For applying Wu's theory, the code is written in Matlab. To discretize the bound vortex sheet we choose 40 points $(x_b(i), y_b(i))$ on the wing of chord-length 2. The bound filaments are chosen to form a cosine-mesh, $\xi_j = \cos\theta_j, \theta_j = j\pi/n$, to provide better resolution and accuracy at the edges. The wing is inclined at an incidence angle of α. We prescribe the free stream velocity U_0, the time step dt and a constant f being the distance from the trailing edge where we put the currently released free filament, also referred to in our theory as $\delta\xi$. The current free vortex is released tangentially to the plate from the trailing edge so that the segment connecting it to the trailing edge will make an angle α with the x-axis.

We will also need some extra points on the wing, namely the centers of the segments connecting two bound vortex points $(x_h(i), y_h(i))$. These midpoints will help us compute the Cauchy's principal value for some integrals later on, which is a very common idea in fluid mechanics.

First, we compute γ_0 knowing the normal imposed velocity on the wing $U_n \sin(\alpha)$. From (32) we can compute γ_0 by a series expansion given in (34). We will stop the iteration when the difference between two such consecutive approximations becomes less than a given ϵ where $0 < \epsilon \ll 1$. The numerical computation of γ_0 is extremely tedious and we will devote our attention to that in the following paragraphs.

We observe that, from (37) we get

$$\gamma_{00}(\xi, t) = -\frac{2}{\pi}\sqrt{\frac{1-\xi}{1+\xi}}\int_{-1}^{1}\sqrt{\frac{1+\xi'}{1-\xi'}}\frac{U_n(\xi', t)}{\xi' - \xi}\,\mathrm{d}\xi'. \tag{55}$$

To find the basic properties of the vorticity γ_{00} distributed over the wing, we take the simple case of a flat plate held at an incidence with $U_n = 1$ by normalization. For this, we are able to compute the integral analytically, as one can see from the solution of the Cauchy integral equation of the first kind.

Lemma 1. *Under the Kutta condition and the integrability condition, the solution of the Cauchy integral equation of the first kind,*

$$\frac{1}{\pi}\int_{-1}^{1}\frac{\phi(y)}{y - x}\,\mathrm{d}y = 1 \text{ is } \phi(y) = \sqrt{\frac{1+y}{1-y}} \quad \forall x \in (-1, 1). \tag{56}$$

According to this lemma, we have

$$\int_{-1}^{1}\sqrt{\frac{1+\xi'}{1-\xi'}}\frac{\mathrm{d}\xi'}{\xi' - \xi} = \pi \quad \forall \xi \in (-1, 1). \tag{57}$$

With this, we see from (55) that γ_{00} (and other γ_{0k}'s) will in general have the square-root factor in front of the integral. Physically, this signifies that the bound vorticity γ_0 generally has an integrable square-root singularity at the leading edge, and vanishes at the trailing edge ($\xi = 1$) as required by the Kutta condition. For this reason, we shall retain the square-root factor from numerical computation until it is finally integrated to give the total circulation.

Thus, the vorticity γ_0 will be computed using (34)–(37) following these steps:

1. From (37) we numerically compute

$$\overline{\gamma_{00}}(\xi, t) = \int_{-1}^{1}\sqrt{\frac{1+\xi'}{1-\xi'}}\frac{U_n(\xi', t)}{\xi' - \xi}\,\mathrm{d}\xi' \text{ for } \gamma_{00}(\xi, t) = -\frac{2}{\pi}\sqrt{\frac{1-\xi}{1+\xi}}\overline{\gamma_{00}}(\xi, t), \tag{58}$$

   in which the square-root factor of γ_{00} is retained as just explained.
2. Substituting (58) in (36) yields

$$G_0\gamma_{01} = -\frac{1}{2\pi}\int_{-1}^{1} g(\xi', \xi)\gamma_{00}\,\mathrm{d}\xi' = \frac{1}{\pi^2}\int_{-1}^{1} g(\xi', \xi)\sqrt{\frac{1-\xi'}{1+\xi'}}\overline{\gamma_{00}}(\xi')\,\mathrm{d}\xi' \equiv U_{n1}, \tag{59}$$

   which is for computation. Here, the term U_{n1} is introduced to form a recursive algorithm pattern in analog with U_n in (37).
3. Inverting (59) using (36) and (37) gives

$$\gamma_{01}(\xi, t) = -\frac{2}{\pi}\sqrt{\frac{1-\xi}{1+\xi}}\int_{-1}^{1}\sqrt{\frac{1+\xi'}{1-\xi'}}\frac{U_{n1}(\xi', t)}{\xi' - \xi}\,\mathrm{d}\xi' \equiv G_0^{-1}U_n^1, \quad (-1 < \xi < 1) = -\frac{2}{\pi}\sqrt{\frac{1-\xi}{1+\xi}}\overline{\gamma_{01}}(\xi),$$

$$\overline{\gamma_{01}}(\xi) = \int_{-1}^{1}\sqrt{\frac{1+\xi'}{1-\xi'}}\frac{U_{n1}(\xi', t)}{\xi' - \xi}\,\mathrm{d}\xi',$$

   of which only $\overline{\gamma_{01}}$ is for numerical computation, just like $\overline{\gamma_{00}}$ in (37).

4. Continuing as in step 2, we compute U_{n2} from (36) to give

$$G_0\gamma_{02} = \frac{1}{\pi^2}\int_{-1}^{1} g(\xi',\xi)\sqrt{\frac{1-\xi'}{1+\xi'}}\overline{\gamma_{01}}(\xi')\mathrm{d}\xi' \equiv U_{n2}. \tag{60}$$

5. Again as in steps 1 and 3 we invert the operator G_0 to give

$$\gamma_{02} = -\frac{2}{\pi}\sqrt{\frac{1-\xi}{1+\xi}}\overline{\gamma_{02}}(\xi), \quad \overline{\gamma_{02}}(\xi) = \int_{-1}^{1}\sqrt{\frac{1+\xi'}{1-\xi'}}\frac{U_{n2}(\xi',t)}{\xi'-\xi}\,\mathrm{d}\xi'. \tag{61}$$

This procedure can be continued indefinitely to give us, finally, Γ_{0k} by integration as

$$\Gamma_{0k} = \int_{-1}^{1}\gamma_{0k}(\xi)\,\mathrm{d}\xi = -\frac{2}{\pi}\int_{-1}^{1}\sqrt{\frac{1-\xi}{1+\xi}}\overline{\gamma_{0k}}(\xi)\,\mathrm{d}\xi, \quad (k=0,1,2,\ldots). \tag{62}$$

The algorithm delineated above has been coded by writing three Matlab procedures or functions, with the first for computing the smooth kernel $g(\xi',\xi)$, the second for $\overline{\gamma_{0k}}$ and the third for U_{nk}. Now we will show how they are computed.

For the kernel $g(\xi',\xi)$ from (33) we place ξ at the midpoint of each grid and ξ' at the bound vortex point. We used finite differences to compute $\mathrm{d}z/\mathrm{d}\xi$ with an explicit form of the real part of the complex quantity.

Computing $\overline{\gamma_{0k}}$ on midpoints gets a bit trickier since by simply applying the trapezoidal rule in computing the integral we get very poor results. We say poor here because we can always compare our result, for some constant velocity U_{nk}, with the result given by Lemma 1 to serve as a standard reference. Therefore, we choose another way, commonly used in lifting flow problems, changing the variable $\xi = \cos y$ to get

$$\overline{\gamma_{0k}}(\xi) = \int_{-1}^{1}\sqrt{\frac{1+\xi'}{1-\xi'}}\frac{U_{nk}}{\xi'-\xi}\,\mathrm{d}\xi' \tag{63}$$

$$= \int_{0}^{\pi}(1+\cos y')\frac{U_{nk}}{\cos y'-\cos y}\,\mathrm{d}y' \equiv \overline{\gamma_{0k}}(\cos y). \tag{64}$$

This now will be solved using trapezoidal rule for points y' and y between 0 and π so that they correspond to the bound points on the wing and to the midpoints, respectively. This method gives a very accurate computational result for the above integral since we do not have to deal with the square root singularity anymore.

Likewise, for $U_{n,k+1}(\xi,t)$, making the same change of variable (see (60) for $k=1$) gives

$$U_{n,k+1}(\cos y,t) = \frac{1}{\pi^2}\int_{0}^{\pi}(1-\cos y')g(\cos y',\cos y)\overline{\gamma_{0k}}(\cos y')\mathrm{d}y', \tag{65}$$

which is computed on the bound points of the wing using again the trapezoidal rule.

We stop the computation whenever the norm of $\overline{\gamma_{0k}}$ falls less than some given ϵ, here with $\epsilon = 10^{-11}$. Adding up all $\overline{\gamma_{0k}}$ we get $\overline{\gamma_0}$ which gives the circulation Γ_0 over the wing by

$$\Gamma_0 = -\frac{2}{\pi}\int_{-1}^{1}\sqrt{\frac{1-\xi}{1+\xi}}\overline{\gamma_0}(\xi)\mathrm{d}\xi, \tag{66}$$

which is computed again using a change of variable as in (65) and then applying the trapezoidal rule. This ends our computation of the quasi-stationary body circulation Γ_0.

5.1.1. Method for computing γ_1

From (41) we get

$$U_{n1}(\xi,t) = \frac{1}{2\pi}\Re\left\{\frac{\mathrm{d}z}{\mathrm{d}\xi}\int_{1}^{\xi_m}\frac{\gamma_w(\xi',t)}{z'-z}\,\mathrm{d}\xi'\right\} = A\gamma_w(1,t)+B, \tag{67}$$

where

$$A = \frac{1}{2\pi}\Re\left\{\frac{\mathrm{d}z}{\mathrm{d}\xi}\int_1^{1+\delta\xi_1}\frac{\mathrm{d}\xi'}{z'-z}\right\},\quad B = \frac{1}{2\pi}\Re\left\{\frac{\mathrm{d}z}{\mathrm{d}\xi}\int_{1+\delta\xi_1}^{\xi_m}\frac{\gamma_w(\xi',t)}{z'-z}\,\mathrm{d}\xi'\right\}, \tag{68}$$

and $\gamma_w(1,t)$ is the vorticity of the latest shed free vortex (the one lying in $1<\xi<1+\delta\xi_1$), which is considered constant on the little gap being just opened in the wake over $\delta\xi_1$ at each time step.

Now using (42) and the linearity of the operators G_0^{-1} and G_1 (and implicitly of G_N) we get

$$\gamma_1(\xi,t) = -G_0^{-1}(U_{n1}+N_1) = -G_0^{-1}[A\gamma_w(1,t)+B+G_N(A\gamma_w(1,t)+B)], \tag{69}$$

$$= -G_0^{-1}(A+G_NA)\gamma_w(1,t) + -G_0^{-1}(B+G_NB), \tag{70}$$

$$= -G_0^{-1}(A+N_{1A})\gamma_w(1,t) + -G_0^{-1}(B+N_{1B}) = \gamma_{1A}\gamma_w(1,t)+\gamma_{1B}, \tag{71}$$

where N_{1A} and N_{1B} have the obvious meaning in accordance with (42). Of course, in (71), γ_{1A} does not represent genuine vorticity, being just a multiplicative factor, but we still denote it by γ for the simplicity of understanding. It becomes clear now how γ_1 is computed: just recall the procedures used in computing γ_0 but this time with $(-A)$ and $(-B)$ instead of U_n to determine γ_{1A} and γ_{1B} and then use the last relation from (71). A and B are computed using the trapezoidal rule. Still, $\gamma_w(1,t)$ is unknown and therefore we have to take our analysis even further.

Using Kelvin's relation for the conservation of circulation (see (51)), i.e. $\Gamma_0+\Gamma_1+\Gamma_w=0$, we get

$$\Gamma_0 + \left[\gamma_w(1,t)\int_{-1}^{1}\gamma_{1A}\,\mathrm{d}\xi + \int_{-1}^{1}\gamma_{1B}\,\mathrm{d}\xi\right] + \left[\gamma_w(1,t)\delta\xi_1 + \int_{1+\delta\xi_m}^{\xi_m}\gamma(\xi,t)\mathrm{d}\xi\right] = 0 \tag{72}$$

where the bound circulation Γ_1 is split into two parts corresponding to A and B, and the wake circulation is also split in two parts, one corresponding to the latest released vortex filament and the second to the rest of the free sheet.

In conclusion, we have

$$\gamma_w(1,t) = -\left\{\Gamma_0 + \int_{-1}^{1}\gamma_{1B}\,\mathrm{d}\xi + \int_{1+\delta\xi_1}^{\xi_m}\gamma(\xi,t)\mathrm{d}\xi\right\}\left(\delta\xi_1 + \int_{-1}^{1}\gamma_{1A}\,\mathrm{d}\xi\right)^{-1}. \tag{73}$$

Here, all the terms are known from our previous discussion. Of course, $\int_{1+\delta\xi_1}^{\xi_m}\gamma(\xi,t)\mathrm{d}\xi$ is known from the conservation of the free circulation from one time step to the next. Hence we know $\gamma_w(1,t)$ and therefore both γ_w and γ_1.

Having the circulation and vorticity on both the bound and the free sheet, we can now compute the convection velocities for the free vortex filaments. These velocities will be computed using relations (25) and (26) in which

$$\Re\left\{\frac{\mathrm{d}z}{\mathrm{d}\xi}\int_{S_b+S_w}\frac{\gamma(\xi',t)}{z'-z}\,\mathrm{d}\xi'\right\} = \frac{\mathrm{d}x}{\mathrm{d}\xi}\int_{S_b+S_w}\frac{(x'-x)\gamma(\xi',t)}{(x'-x)^2+(y'-y)^2}\,\mathrm{d}\xi' + \frac{\mathrm{d}y}{\mathrm{d}\xi}\int_{S_b+S_w}\frac{(y'-y)\gamma(\xi',t)}{(x'-x)^2+(y'-y)^2}\,\mathrm{d}\xi',$$

$$\Im\left\{\frac{\mathrm{d}z}{\mathrm{d}\xi}\int_{S_b+S_w}\frac{\gamma(\xi',t)}{z'-z}\,\mathrm{d}\xi'\right\} = -\frac{\mathrm{d}x}{\mathrm{d}\xi}\int_{S_b+S_w}\frac{(y'-y)\gamma(\xi',t)}{(x'-x)^2+(y'-y)^2}\,\mathrm{d}\xi' + \frac{\mathrm{d}y}{\mathrm{d}\xi}\int_{S_b+S_w}\frac{(x'-x)\gamma(\xi',t)}{(x'-x)^2+(y'-y)^2}\,\mathrm{d}\xi'.$$

Note that these relations also give the normal and tangential velocities. In convecting the free vortices it would be easier though, to work with the x and y components of the velocities. When we discretize the integrals, the sum will contain a $+\delta^2$ in the denominator (the blob) whenever ξ' is on S_w. However, δ is set to zero when ξ' is on S_b. After all these steps, we are ready to go to the next time step and to compute all the required unknowns again.

This ends the description of our method. An example is provided in Fig. 4. The example shows how accurate the method is by zooming inside the vortex. We do not use in this case any point insertion technique just to show how good the raw result is. The numerical implementation uses an advancing wing velocity $U_0=10$, an angle of inclination $\alpha=18^\circ$, a blob $\delta=0.2$ and a fixed time step $\mathrm{d}t=0.0002$, the wing's chord-length being 2. The plot is obtained after 10,000 time-steps, or after the wing traveled 10 chord lengths.

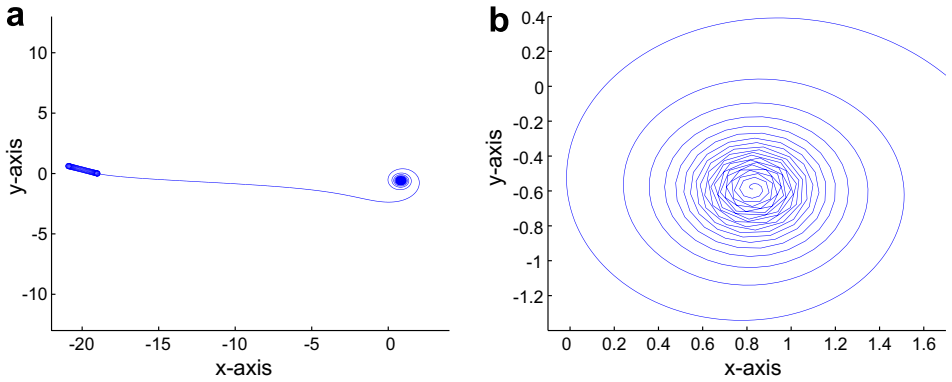

Fig. 4. Wu's method for vortex forming behind a wing flying at $\alpha = 18^\circ$, $U_0 = 10$, time step $dt = 0.0002$ and blob $\delta = 0.2$, the wing's chord length being 2. In figure (b) one can see how accurate the method is when we zoom inside the vortex. Plot after 10,000 time-steps.

6. Comparison of the two methods for the rigid wing

6.1. Comparison between the Results

Both methods produce very nice results. In his papers, Krasny observes that the smaller the blob δ gets, the more accurate his method becomes in terms of capturing the physical effect of viscosity. By that it is understood that we would like to capture better what happens near the center of the vortex, and by decreasing the blob we get more and more roll-ups. We ran similar simulations using Wu's method and we noticed very nice convergence of the inner turns inside the vortex. The plots in Fig. 5 are obtained for a flat plate of chord $c = 2$, inclined at an angle $\alpha = 5^\circ$, traveling 5 chord lengths with a speed $U_0 = 10$. For plot (a) we used a blob $\delta = 0.18$ and a time-step $dt = 0.002$. For plot (b) we decreased both the blob, to $\delta = 0.14$ and the time-step to $dt = 0.001$ and got more roll-ups inside the vortex. For plot (c) we chose an even smaller blob, $\delta = 0.1$ and smaller time-step $dt = 0.0005$ we got a better resolution and more roll-ups inside the vortex. Throughout each of these simulations the time step was maintained constant.

This shows how accurately Wu's method can capture the inner roll-ups when we decrease the time-step and the blob. In a later section, we will analyze the convergence of the outer wake with respect to these two parameters.

Comparing the two methods for identical sets of initial data (see Fig. 6) we can see that Wu's method behaves much better in capturing the roll-ups inside the vortex ring. The modified vortex blob method would produce the same number of roll-ups for a smaller blob which will require a smaller time-step for accuracy and therefore a longer computational time. The plots presented in Fig. 6 are obtained for a flat plate of chord $c = 2$, inclined at an angle $\alpha = 18^\circ$, traveling with a speed $U_0 = 10$, with a time-step $dt = 0.0002$ and after ten thousand time-steps. For both plots, the blob is chosen to be $\delta = 0.2$. No point insertion technique is used in these plots to better see the accuracy of the methods. The plot obtained using Wu's method proves to be very stable for small blobs when the number of roll-ups becomes very big.

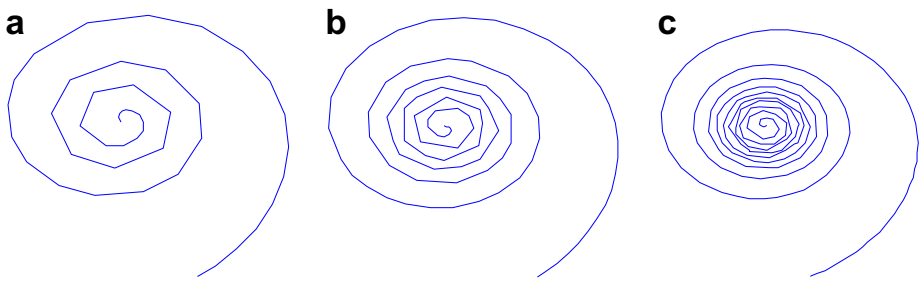

Fig. 5. Wu's method provides better resolution inside the vortex when decreasing the blob and the time-step.

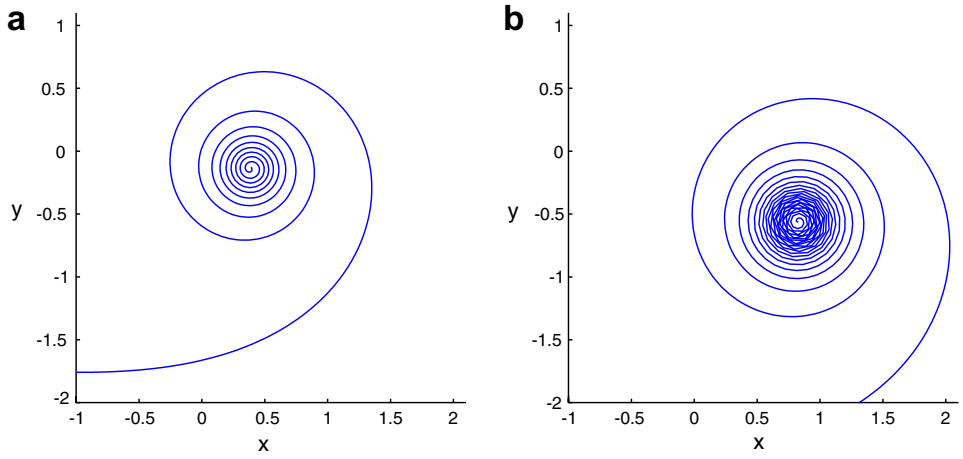

Fig. 6. (a) Vortex obtained with the modified method and (b) vortex obtained with Wu's method.

The difference between the two plots resides, perhaps more importantly, in the position and radius of the vortex ring. The center of the ring obtained with the modified method is located at $(x, y) = (0.395, -0.151)$ while Wu's method gives us a ring with center located at $(x, y) = (0.827, -0.588)$. The radius of the first one is $R = 0.97$ while for the second one the radius is $R = 1.218$. So one can see that by Wu's method we get a slightly bigger vortex ring located a bit lower and more to the right than the one obtained by the other method. To validate the ring dimensions we will refer in the next subsection to experiments performed using a NACA wing. However, we could not find any experiments that would provide us the correct position for the center of the vortex ring. The discrepancy between the two methods regarding this position should be settled by well-performed experiments for the final say.

6.2. Validating the numerical computations

6.2.1. Radius of the vortex

One of the few experiments we could find in the literature involving the structure and development of a tip vortex shed from a conventional wing is that performed in 1996 by Devenport ([3]). His experiments were performed in the Virginia Tech Stability Wind Tunnel and a rectangular-planform NACA 0012 wing with a 0.203 m chord, and a blunt tip was used to generate the vortices. The measurements we are going to refer to were done with a chord Reynolds number $U_\infty c/\nu$ of 530,000 (corresponding to a velocity of about 37.3 m/s) with the wing at an angle of attack α of 5°. Devenport's results were taken at cross-sections $5c$, $10c$, $15c$, $20c$, $25c$ and $30c$ downstream of the wing leading edge (here c represents the wing chord length). He showed using these six points of data that the scale of the spiral grew approximately as the square root of the distance traveled by the wing (see [3, Fig. 9, pp. 84]).

Even though the difference between this experiment and our numerical model is obvious (NACA wing has thickness), Devenport's results are as close as possible to our model, and by comparison we can demonstrate that our model and method are indeed valid approximation of real-life physics.

The simulation using Wu's method is performed with the following characteristics: a chord length $c = 2$, an advancing speed of 10, an angle α of 5° to match Devenport's experiment, a blob of 0.2 and a time-step of 0.0005. The wing is left to travel for 12,000 time steps which corresponds to 30 chord lengths and the sample of data for the behavior of the radius is taken after every 100 time-steps or every quarter-chord-length traveled. The radius is measured, for both the experimental and numerical results, from the center of the vortex (considered to be the location of the first filament released) to the right-most point of the wake.

The results are very accurate, and the large number of data points taken offers a very detailed view of the agreement with the experiment. In Fig. 7a, we can see that the behavior of the radius in time mimics very well the behavior of the square-root function represented by a dotted line. The slight discrepancy at the beginning of the motion could be due to the fact that we miss thickness in our model. On the other hand, the behavior of

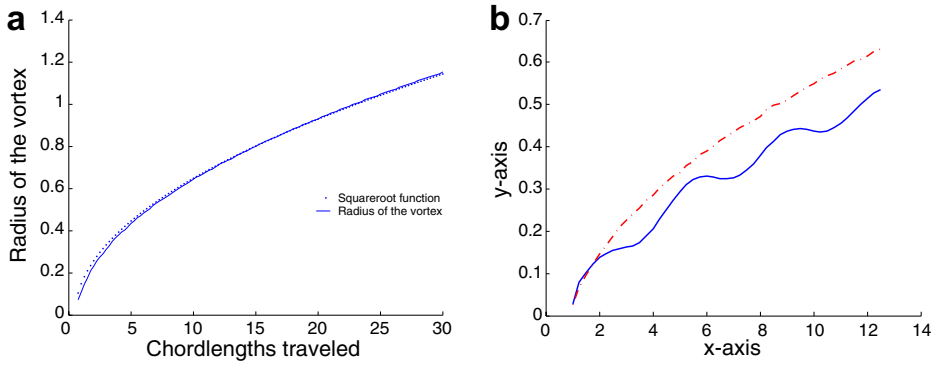

Fig. 7. (a) Plot of Wu's radius of the vortex versus the square-root function. Here, the x-axis represents the number of chord-lengths traveled by the wing and (b) comparison of the behavior of the radius growth for Wu's method (dot-dashed line) and the modified vortex blob method (solid line).

the radius in the modified vortex blob method (see the solid line in Fig. 7b), is quite far from Wu's case (the dot-dashed line in Fig. 7b) and consequently from the observations made by Devenport.

These experiments were run on a Pentium 4, 3.0 GHz box and on average the amount of time needed to complete the simulations using Wu's method was 10% higher than when using the other method. This is due to the complexity of Wu's calculations but the price is paid for a good reason, since this complexity brings a better resolution of the vortex core as seen in the previous section.

7. Results obtained for nonlinear motions

Some very interesting cases to be analyzed in the following sections are those for heaving and pitching motions. While the heaving or fluttering motion is closer to that of a bird's wing in flight, the pitching motion is better related to the movement of a fish's fin. Since both movements have very close correspondents in nature we will try to see how our method compares with the experiments found in the literature. Nevertheless, we will try to argue that they do provide thrust, and, in the case of a mixed heaving and pitching motion, we will try to describe which kind of flight generates lift and which generates thrust.

7.1. Wu's method for heaving motion

The fluid mechanics literature is richer in experiments involving a heaving wing. Some experiments were done by Bratt in 1953 (see [1]) and more recently by Jones et al. in 1998 (see [6]) and by Lai et al. in 2002 (see [12]). To further validate our unsteady method and ascertain its limits of applicability, the unsteady wake structures numerically generated are compared with the wake structures found experimentally.

If we consider a flapping wing and denote by $V_p = hk$ the non-dimensional plunging velocity, where h is the heaving amplitude in terms of the chord c and k is the reduced frequency $\omega c/U_0$, then it is well known from the above experiments that in viscous fluids, stationary airfoils and airfoils plunging sinusoidally with low V_p generate viscous related drag. As the V_p is increased the drag is reduced and eventually thrust is produced. However, the potential-flow code predicts zero drag for a stationary airfoil and thrust for a plunging airfoil at any finite frequency. Therefore, qualitative and quantitative comparisons of the wake structures are made for a sufficiently big V_p such that the experiment will show a thrust mode as well. The qualitative agreement demonstrated in Fig. 8a is excellent, in which the numerical plot is the lower image and the experiment of ([12]) is the center strip. In the experiment, the distance between the centers of the vortices in the second pair of vortices is about 0.4 when the plate length is 1 while for the computational result, the same distance is 0.8 for a plate of length 2. For the numerical plot we use a foil advancing to the left in a stationary flow, flapping at 10 Hz with a non-dimensional plunge velocity of $V_p = 0.076$ which perfectly match the experimental data. The amplitude is $h = 0.038$ and the wing velocity is $U_0 = 5$. Here, a small blob is used, i.e. $\delta = 0.11$, the time step is $\Delta t = 0.001$ and the execution is stopped after 2630 time steps. The experiment was conducted by Lai

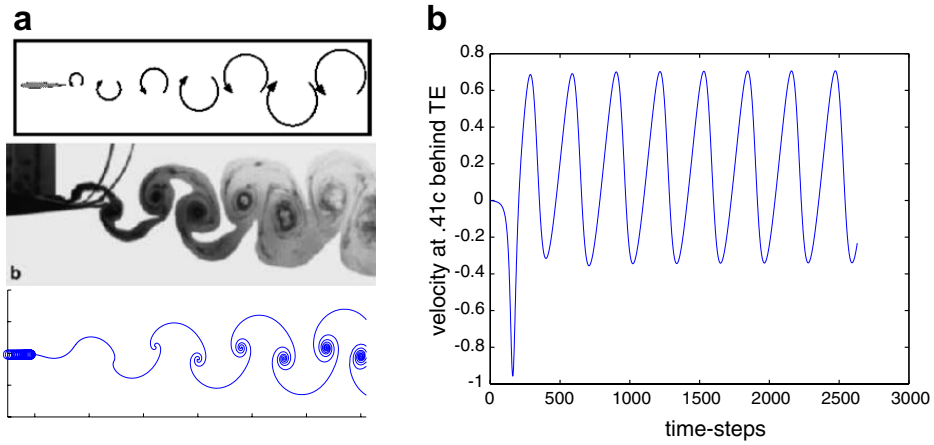

Fig. 8. (a) Heaving wing; Upper: rotational orientation of eddies; Center: experiment done by Lai in 2002; Lower: Wu's numerical method and (b) Heaving wing; profile of the velocity at $0.41c$ downstream behind the trailing edge.

et al. in the water tunnel facility at the Department of Aeronautics and Astronautics, Naval Postgraduate School, Monterey, California.

The upper image shows a schematic illustration of the sense of rotation of the eddies. This pattern of trailing vortices will obviously generate thrust, since they will induce a jet spreading toward downstream (as will be shown numerically below), hence a positive thrust results by momentum argument. To exhibit the basic mechanism underlying the wake momentum for producing thrust, we analyze the velocity profile at a point located at $0.41c$ behind the trailing edge. To better capture the thrust production we should have integrated this profile along a $x = ct$. section; however, this punctual analysis of the well spread wake momentum should give a good interpretation of the thrust. One could see from Fig. 8b that the mean velocity at this point is positive, indicating the presence of a jet directed downstream. This shows how important the study of the wake is, the released vortices being able to create thrust and therefore to move the bird or the fish forward.

The first drop in the velocity which makes it negative is due to the beginning of the motion, however, after the first quarter of the motion period, thrust will be generated. For physical interpretation, this represents the period before the flow particles situated at $0.41c$ downstream from the trailing edge get influenced by the disturbance created by the heaving wing.

7.2. Pitching motion

A different wake in contrast with that trailing a wing in heaving motion is produced by a wing in pitching motion (see Fig. 9). Here, the upper part represents the plot obtained by Wu's method while the lower one

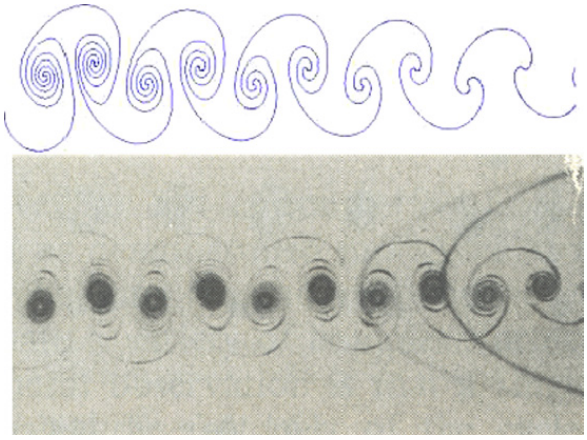

Fig. 9. Pitching motion of a wing advancing from the left to right; Upper: Wu's numerical method; Lower: experiment by Koochesfahani in 1989.

represents the experiment done in 1989 by Koochesfahani (see [10]) at Caltech. This time the wing is advancing from the left to right having a high frequency ($f = 5$ Hz $\Rightarrow \omega = 2\pi f \approx 31.14$) of pitching about an axis at the quarter-chord point in match with the experimental conditions. The amplitude is $\pm 2°$ and the advancing speed is 10, the chord-length being 2. The blob is $\delta = 0.2$, the time step $\Delta t = 0.0005$ and the procedure is stopped after 3000 time steps. Again the comparison shows a very accurate behavior compared with the experiment. The position and orientation of the vortices in the wake suggest a jet-like wake behind the pitching foil. Koochesfahani shows though, that at low frequencies in real flow, the drag effect is dominant due to the viscosity. This could be a research door for the biologists to see what kind of frequencies exist in the case of rapid fish movements and how they agree with the numerical and water tank experiments.

7.3. Mixed pitching and heaving motion

A bird wing is an airfoil combining the functions of an aircraft wing and propeller blade to produce lift and thrust. This is done by a mixed wing motion involving both heaving and pitching. This more complex movement is very nonlinear and we'll try to analyze it using Wu's method.

Just to see the shape of the wake behind a wing performing a mixed motion, we use Wu's method for the following case (see Fig. 10a): a heaving movement with amplitude $h = 0.038$ and angular frequency $\omega_h = 8$ combined with a pitching about an axis at $x_c = 0.15$ from the leading edge, with amplitude of 3° and angular frequency of $\omega_p = 8$. The wing starts from rest, lying on the $[-1, 1]$ segment of the Ox axis, with zero phase difference between heaving and pitching. It also moves to the left with a speed $U_0 = 3.12$ and with a vortex element shed into the wake after every time step $\Delta t = 0.002$. The plot is made after 2000 time steps.

However, we want to describe more realistically the actual movement of a bird's wing. For that, we have to take into consideration some more aspects from the natural movement. We know that in order to generate lift and thrust, the down-stroke and the upstroke of a bird's wing are not similar. The down-stroke is more powerful by keeping the wing section almost horizontal, while in the upstroke the wing is inclined, having the trailing edge lower than the leading edge. We will show that this movement generates lift and therefore we will call this ascending flight. However, a wing which does not incline for the upstroke, i.e. having a pure heaving

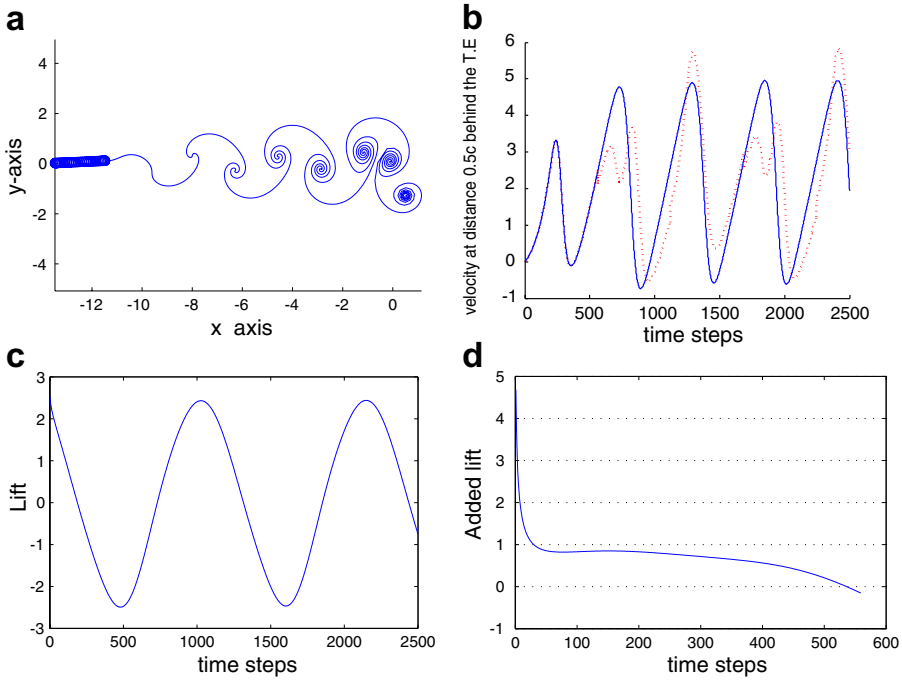

Fig. 10. Wu's method for a mixed heaving-pitching motion: (a) An example of mixed heaving-pitching motion; (b) comparison of flow velocities at a distance $0.5c$ behind T.E. for cruising flight (solid line) and ascending flight (dotted line); (c) lift for cruising flight; and (d) added lift for two half-periods for ascending flight.

motion, will not create any lift because of the symmetry of this motion. Without considering the bird's weight, we could argue that this kind of motion will keep the bird at a constant altitude and we will show that it generates more thrust than the first motion. Therefore, we will call this cruising motion.

To better see the difference between these two movements, we analyze them using Wu's method. The ascending motion is composed of a heaving with amplitude $h = 0.425$ and angular frequency $\omega_h = 8$. While for the down-stroke we have only this heaving motion, for the upstroke we combine it with a pitching motion. Thus, when the wing starts the upstroke, we start to incline it with an amplitude $\theta_0 = 4°$ and an angular frequency $\omega_p = 8$ equal to that of the heaving so that when the wing ends the upstroke it will find itself again in a horizontal position.

The cruising flight is modeled using a pure heaving motion with the same characteristics as above. For both motions we pick a flight velocity of $U_0 = 8$ and a time step for the numerical method with $\Delta t = 0.0007$. The blob is $\delta = 0.2$ and the pitching motion is realized around the trailing edge. The lift is computed as in Section 7.7.

Fig. 10b shows the velocity of a particle located at a distance $0.5c = 1$ behind the trailing edge. Since the fluid is stationary and only the wing is moving, we can see that, having a positive average velocity behind the trailing edge, thrust will be generated in both cases. However, one will notice that in the case of cruising flight (the solid line) more thrust is generated than in the case of ascending flight. For instance, during the half-period corresponding to the upstroke, the thrust for the cruising motion is 20% larger than the other one which makes this motion more suitable when the bird wants to advance. However, if we take a look at the lift, we will see that, due to the symmetry of the motion, the overall lift in the case of a cruising flight is practically zero (see Fig. 10c). Not the same thing can be said about the ascending case. In this case, if we add up the lift produced during the upstroke and the one produced during the down-stroke we will see that the resulting lift is quite relevant (see Fig. 10d).

In conclusion, we have demonstrated that these two types of mixed motions provide quite different results: the cruising movement produces thrust but no lift while the ascending one produces less thrust but considerable lift. It is worth mentioning though, that in a real flight things change a bit. To be able to support its own weight, the bird will use some pitching even during cruising so that the generated lift will cancel this new force. Also during the ascending flight, the amplitude of pitching will have to increase because of the same reason.

Another fact observed in nature is that on the upstroke of the wing beat, the feathers at the end of many bird wings twist sideways to let the air slip through with little resistance. This will increase even more lift compared to the pure heaving motion.

7.4. Bending motion

In this subsection, we attempt to demonstrate the ability of Wu's method in dealing with nonlinearity. We use an example of a plate with zero thickness but having a variable camber. The incidence angle of the chord is

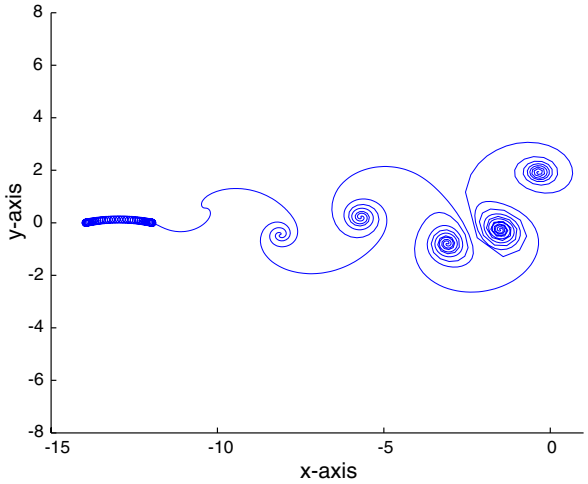

Fig. 11. Wu's method for a bending motion.

zero but there is an actual incidence angle given by the camber. The deformation of the wing used in Fig. 11 is given by $y = \epsilon(1 - x^2)$, with the amplitude $\epsilon = (1/8)\sin(\omega t)$. The angular frequency is $\omega = 8$, the advancing speed $U_0 = 6$, the time step $\Delta t = 0.002$ and the blob $\delta = 0.2$. The plot is obtained after 1100 time steps and very accurately catches the formation and structure of the wake vortices.

This example has very nice applications when combined with a flapping motion. In that case, it would describe the motion of a wing composed by a flexible membrane like the one found in bats (*Chiroptera*) or in some insects.

7.5. Analysis of the first released vortex element

To better understand the differences between the two methods as noted, we analyze the first released vortex element for a rigid wing (of chord-length 2) advancing at a given angle of attack. We are able to compute the circulation of this first vortex analytically and therefore to compare this exact circulation with the ones given by the two computational methods.

The analytical formula for the 'quasi-steady' vorticity (γ_0) on the body without any wake effect is given by equation (39) after a simple change of variables. The vorticity on the wake (γ_w) is computed using Eq. (52) along with Lemma 1. Finally, the vorticity (γ_1) induced on the body by the wake is computed from formula (45). (For more details please consult [8]). When the wing goes abruptly from horizontal position to an incidence angle α so that the wake-free circulation on the body is $\Gamma_0 = 1$, we have the following formulas for the discussed vorticities

$$\gamma_0 = \frac{1}{\pi}\sqrt{\frac{1-x}{1+x}}, \quad (-1 < x < 1), \tag{74}$$

$$\gamma_w = -\frac{1}{\pi}\sqrt{\frac{1}{2(1+Ut-x)}}, \quad (1 < x < 1 + Ut, Ut \ll 1), \tag{75}$$

$$\gamma_1 = -\frac{1}{\pi}\frac{1}{\sqrt{(1+x)(1+Ut-x)}}, \quad (-1 < x < 1, Ut \ll 1). \tag{76}$$

In Fig. 12, we plot these functions without the $1/\pi$ factor for a starting vortex placed at a distance of 0.1 behind the trailing edge. A couple of things can be observed from this plot. Firstly, we can see that both γ_0 and γ_1 are unbounded at the leading edge of the wing which is in accordance with the known wing theory results. The more important aspect, however, is the finding that the starting vorticity in the wake also has a square-root singularity at $\xi_m = 1.1$, the downstream end of the wake. Therefore, one should be very careful on the numer-

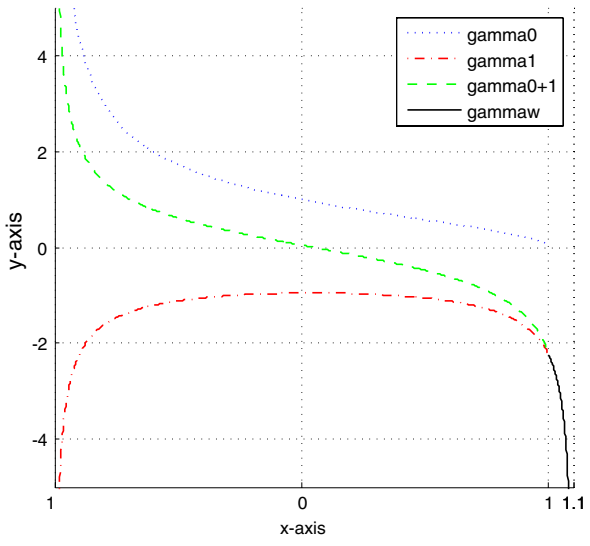

Fig. 12. Plot of the vorticity functions for one released vortex filament.

ical analysis of this first wake vorticity. In fact, the strength of Wu's method resides exactly in this combination of analytical and numerical methods used to catch the behavior of the wake near the trailing edge. In contrast, the modified vortex blob method considers this very first released element as an extension of the body, computing its circulation purely numerically by inverting a linear system.

This can be seen better when comparing the results given by the two methods with the analytical result. For a wing advancing with a speed $U_0 = 10$, at an angle of 18°, and the wake circulation computed after the wing traveled a distance of 0.005, the analytical wake circulation from equation (75) is $\Gamma_w = -0.61804$, the same circulation computed with Wu's method is $\Gamma_w = -0.6510$ and the one computed using the modified vortex blob method is $\Gamma_w = -0.7131$. Such a discrepancy will be propagated in the wake later, and this is why we are seeing much better results for Wu's method.

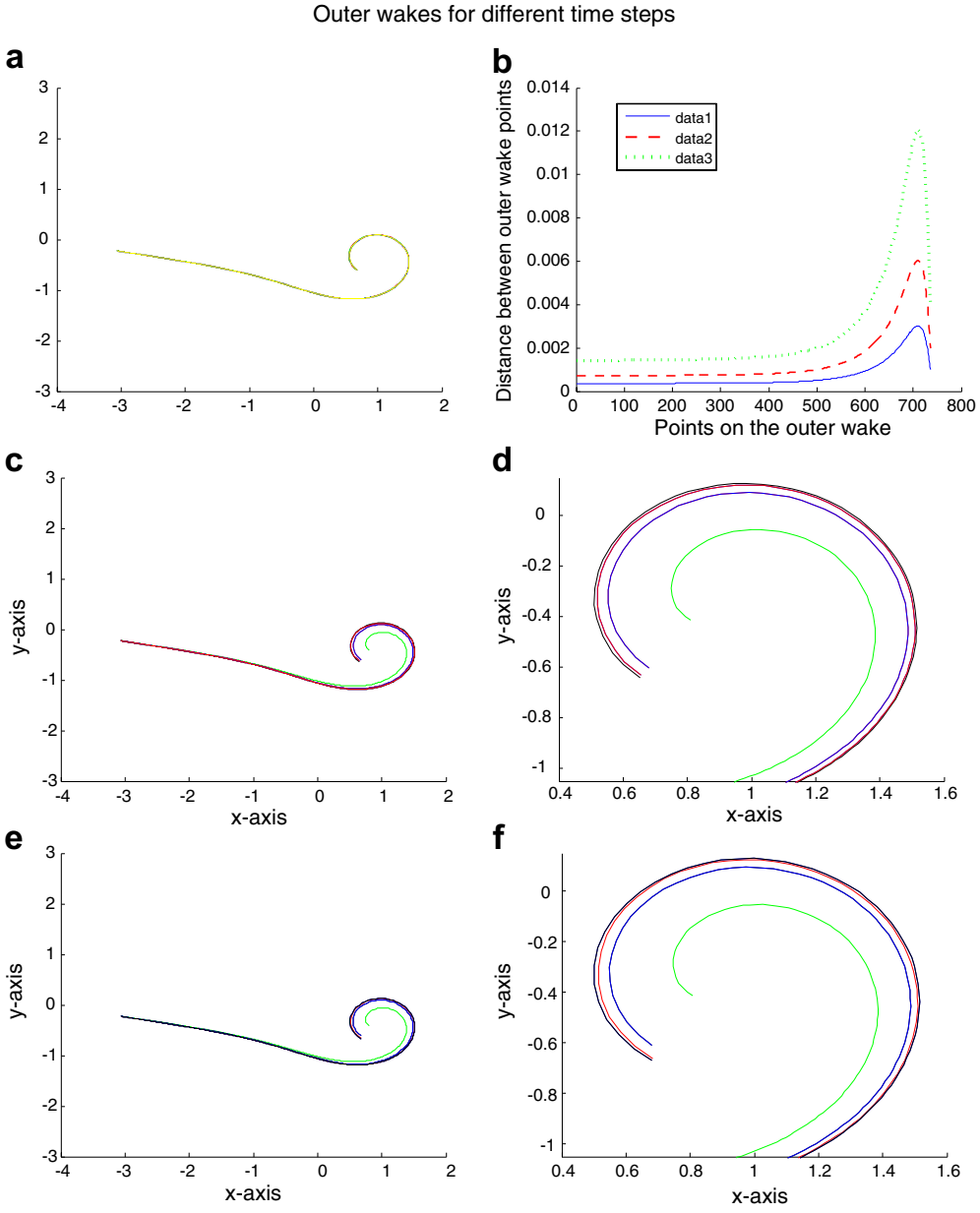

Fig. 13. (a) The outer wake; (b) distances between points on the wakes for a constant blob but variable time step; (c) and (d) Outer wake and a zoom for a constant time step $dt = 0.000125$ but variable blob; (e) and (f) Outer wake and a zoom for a constant time step $dt = 0.0005$ but variable blob. For plots (c), (d), (e) and (f) going from the innermost wake to the outermost one we have $\delta = 0.4$, $\delta = 0.2$, $\delta = 0.1$ and $\delta = 0.05$.

7.6. Convergence analysis

We demonstrate the accuracy of Wu's method by conducting a convergence study of the outer wake both with respect to time and blob. The outer wake represents a cut of the whole wake as it is depicted in Fig. 13a.

For a blob size of 0.2 we vary the time step, choosing $dt = 0.0005$, 0.00025, 0.000125, and 0.0000625. We stop our computation after 1000, 2000, 4000, and 8000 steps, respectively. This implies that the wing travels the same distance but we have more points in the wake, or a finer mesh in other words. We compute the distance between the resulting outer wakes by computing the distance between corresponding points on these wakes. In Fig. 13b, we can see a plot of these distances. The dotted line represents the point distances between the outer wakes with $dt = 0.0005$ and $dt = 0.00025$, the dashed one the point distances between the outer wakes with $dt = 0.00025$ and $dt = 0.000125$, while the solid one corresponds to the point distances between the outer wakes with $dt = 0.000125$ and $dt = 0.0000625$. It is obvious how these distances decrease as time step decreases. More than that, the average distance between the outer wakes are 0.0028, 0.0014 and 0.0007 going from the coarsest mesh to the finest. This shows how the outer wake converges with respect to time step.

We perform a similar convergence study by varying the blob size. For a time step of 0.000125 and 4000 time steps we choose the blob size to be 0.4, 0.2, 0.1 and 0.05. Again we compute the distance between the points on the outer wake and it turns out that the average distance between these points goes from 0.0250 to 0.0057 and to 0.0015. Hence, the method is convergent with respect to the blob size. A representation of these outer wakes can be seen in Fig. 13c with a zoom of the outer part of the vortex in Fig. 13d. Here, as we go from the innermost roll-up to the outermost one, the plots correspond to $\delta = 0.4$, $\delta = 0.2$, $\delta = 0.1$ and $\delta = 0.05$.

We go even further and do the same computations for a different time step, $dt = 0.0005$ and 1000 points in the wake. This case is similar to the one above in terms of the distance traveled by the wing. The blobs are again the same. The results show that the distances between the outer wakes are 0.0253, 0.0062 and 0.0027, respectively. Again, a representation of these outer wakes can be seen in Fig. 13e with a zoom of the outer part of the vortex in Fig. 13f. Again, as we go from the innermost roll-up to the outermost one, the plots correspond to $\delta = 0.4$, $\delta = 0.2$, $\delta = 0.1$ and $\delta = 0.05$.

It can be seen that in this case, for a bigger time step, the convergence is slower in δ. In other words, if we choose our blob size carefully, by decreasing the time step we will get a faster convergence of the outer wake. This shows that our method is more dependent on the time step than on the blob itself.

Some other experiments that are not included here show the dependence of the methods to the incidence angle. These experiments demonstrate that for a given time, for both methods the wake flattens more and more as we decrease the angle, approaching the horizontal. Of course, this is an expected result since for a plate advancing at a zero angle of attack we expect to get a linear wake.

Another experiment tries to feed the first n vortex elements (where n is 30, 50, 100) from Wu's method into the modified vortex blob method hoping that these points, having less error near the trailing edge, will correct the modified method and will produce an outer wake closer to the one given by Wu's. The experiment is not very conclusive because of the effect the core of the vortex has on the outer wake. Unfortunately, by feeding all these points from one method to the other, the accuracy is lost in the center of the vortex and this chaotic behavior affects the whole wake.

To show how the methods converge to a common result for the outer wake after we minimize the impact of the error introduced in the first released vortex element, we also try to make the initial jump of the plate from the horizontal to angle α smoother. This experiment again does not prove to be very successful since, after all, we end up adding the contribution of all the smaller steps and the total error introduced in the wake is almost the same as in the non-smooth case.

7.7. Verifying Wagner's result

A validation of Wu's method and of the numerical method may be given by Wagner's [28] classical problem for a flat plate airfoil making a time-step increase in incidence angle so that $\Gamma_0(t) = H(t)$, the unit Heaviside step function. With the nonlinear terms dismissed, equation (52) reduces in the linear limit to

$$\int_1^{1+Ut} \gamma_w(\xi,t)\sqrt{\frac{\xi+1}{\xi-1}}\,d\xi = -1, \quad (t>0), \tag{77}$$

with γ_w properly scaled to have the unit change of the integral as a standard. Using the results of Kármán and Sears [8], we change the variable $s = 1 + Ut - \xi$, so that $\gamma_w(\xi,t) = \gamma(1+Ut-s,t) = \hat{\gamma}(s,t)$, s being the distance measured along $S_w(t)$ from the tip of the starting vortex (at $\xi = \xi_m$) backward toward the trailing edge, by which (77) becomes

$$\int_0^{Ut} \hat{\gamma}(s,t)\sqrt{\frac{2+Ut-s}{Ut-s}}\,ds = -1, \quad (t>0). \tag{78}$$

We are interested in the beginning of the motion and therefore $0 \leqslant Ut - s < Ut \ll 1$, so the leading order of the small-time asymptotic representation of (78) is

$$\int_0^{Ut} \hat{\gamma}(s,t)\sqrt{\frac{2}{Ut-s}}\,ds = -1, \quad (0 < Ut \ll 1). \tag{79}$$

But now this is Abel's integral equation and it has the solution

$$\hat{\gamma}(s,t) = -(\pi\sqrt{2s})^{-1}, \quad (Ut \ll 1). \tag{80}$$

Again following Kármán and Sears [8], Wagner's lift-deficiency function $\Phi(Ut)$ yields

$$\Phi(Ut) = -\int_1^{1+Ut} \frac{\gamma(\xi)}{\sqrt{\xi^2-1}}\,d\xi = -\int_0^{Ut} \frac{\hat{\gamma}(s)}{\sqrt{2(Ut-s)}}\,ds = \frac{1}{2}, \quad (\text{as } t \to 0), \tag{81}$$

which is Wagner's result, stating that an impulsively started flat-plate airfoil generates instantly half the final lift, the latter of which the wing eventually achieves, i.e. $1 - \Phi(Ut) \to 1$ as $t \to \infty$, which is known as the Wagner effect.

The designed numerical method is used to compute the initial lift and the lift at every later time step. After a sufficiently long time the lift is considered to be $L(t=\infty)$ or the final lift. The plot is presented in Fig. 14. The result is obtained with blob 0.2, speed 10, time step 0.001 angle of attack $\alpha = \pi/20$ and the final lift considered after the wing has traveled $8k$ time steps or approximately 40 chord lengths.

We compute the lift using the theory in ([8]). Sears shows how the total momentum of continuously distributed vortices (consisting of the airfoil and its wake) is

$$I = \rho\int_{-1}^{1} \gamma(x)x\,dx + \rho\int_1^{\xi_m} \gamma(\xi)\xi\,d\xi. \tag{82}$$

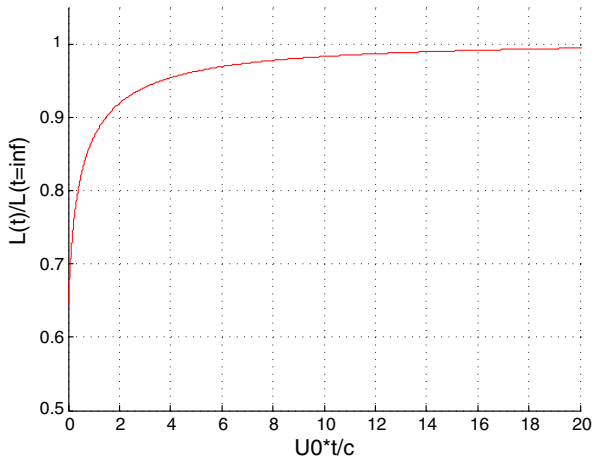

Fig. 14. Variation of lift after the initiation of a sudden forward motion of a two-dimensional flat plate.

Using the fact that the lift is given by $L = -\mathrm{d}I/\mathrm{d}t$, the decomposition of vorticity $\gamma(x) = \gamma_0(x) + \gamma_1(x)$ and Kelvin's theorem of conservation of circulation, we obtain

$$L(t) = -\rho \frac{\mathrm{d}}{\mathrm{d}t} \int_{-1}^{1} \gamma_0(x)\mathrm{d}x + \rho U \Gamma_0 + \rho U \int_{1}^{\xi_m} \frac{\gamma(\xi)\mathrm{d}\xi}{\sqrt{\xi^2 - 1}}, \tag{83}$$

where the first term represents the contribution of the apparent mass, the second one the quasi-steady lift, and the last one the lift given by the wake. The apparent mass behaves like a delta function of time centered at zero (γ_0 is constant after $t = 0^+$) and we will explain in more detail how we compute the main contribution of this term. We will compute $L(t)/\rho U$, from which we can deduce the ratio $L(t)/L_\infty$, with L_∞ given by setting $\xi_m = \infty$ in the expression for $L(t)$.

This is how we compute the contribution of the apparent mass: since this contribution comes only from a very small time interval around $t = 0$, we consider the first time step a bit bigger, $\mathrm{d}t_1 = 0.05$. In this time interval we compute the apparent mass analytically by linearly varying the angle of attack from 0 to $\alpha = \pi/20$. As a consequence, we get

$$-\frac{1}{U}\frac{\mathrm{d}}{\mathrm{d}t}\int_{-1}^{1}\gamma_0(x)\mathrm{d}x = \frac{2}{U}\frac{\mathrm{d}}{\mathrm{d}t}\int_{-1}^{1} U_n\sqrt{\frac{1-x}{1+x}}\mathrm{d}x = 2\cos(\alpha(t))\alpha'(t)\int_{-1}^{1}\sqrt{\frac{1-x}{1+x}}\mathrm{d}x, \tag{84}$$

where $\alpha'(t)$ is the slope of the linear function going from 0 to $\pi/20$ in the interval $\mathrm{d}t_1$.

This is indeed a very nice way of verifying Wagner's result and it can be seen that the theoretical result (initial lift is half the final lift) and the numerical one (about 0.64) are very close and that our numerical result is significantly better than some other ones. For instance, Katz and Plotkin [7] get a result of about 0.85. Again, this demonstrates the robustness of Wu's method.

7.8. Analyzing the lift for an abrupt Heaviside flexible motion and an abrupt Fourier flexible motion

Our theory has been applied above to illustrate nonlinear effects in several aspects of unsteady lifting locomotion, with objectives focused on one central issue at a time. It is of new significance to extend Wagner's classical problem to include an abrupt Heaviside flexible motion of the wing to pursue studies on the nonlinear effects of two different origins and further on their mutual interaction. Thus, the new problem is that at time $t = 0^-$ the wing coincides with the segment $[-1, 1]$ on the Ox-axis and at time $t = 0^+$ the wing undergoes a stepwise transformation into a parabolic wing with $x(\xi) = \xi, y(\xi) = \epsilon(1 - \xi^2) \forall \xi \in [-1, 1]$ plus a rotation to an angle of incidence α about the trailing edge, so that the wing assumes the following new shape function:

$$X = 1 + \epsilon(1 - \xi^2)\sin(\alpha) - (1 - \xi)\cos(\alpha), \tag{85}$$

$$Y = \epsilon(1 - \xi^2)\cos(\alpha) + (1 - \xi)\sin(\alpha). \tag{86}$$

Hence, the outer normal will be given by $\mathbf{n} = (2\epsilon\xi\cos(\alpha) + \sin(\alpha), -2\epsilon\xi\sin(\alpha) + \cos(\alpha))$. Furthermore, the normal component of the fluid velocity becomes

$$U_n = U_\infty\{2\epsilon\xi\cos(\alpha) + \sin(\alpha)\}(1 + 4\epsilon^2\xi^2)^{-1/2}. \tag{87}$$

Again, we get a very nice resolution of the vortex core (see Fig. 15a) while the behavior of the lift can be seen in Fig. 15b. The plots are obtained for deformation $\epsilon = 0.05$, angle of attack $\alpha = \pi/18$, blob $\delta = 0.2$, flow velocity $U_0 = -3.12$, time step $\mathrm{d}t = 0.002$ and 10^3 time steps. This corresponds to the wing traveling 10 chord lengths to the left. The amplitude of deformation ($\epsilon = 0.05$) will give an effective angle of attack of approximately $\pi/18 + \pi/36 = \pi/12$ or 15°. The plot of the lift shows that in this case the initial lift would be about 0.72 of the final lift (see Fig. 15b) for this generalization of Wagner's result.

For the Fourier movement, the equation of the motion is similar to the one in the Heaviside case except that now, the amplitude of the deformation is variable, i.e. $\epsilon = \epsilon(t)$ where $\epsilon(t) = \epsilon_0\cos(\omega t)$. The equations given above will remain the same with this change. For the numerical simulations we chose $\epsilon_0 = 0.2$ and $\omega = 5$ so that after 1256 time steps (see Fig. 16a) the 2π period of the cosine has been covered. At a time step of $\mathrm{d}t = 10^{-3}$ and a flow velocity of $U_0 = -3.12$ this corresponds to 2 chord lengths of flight.

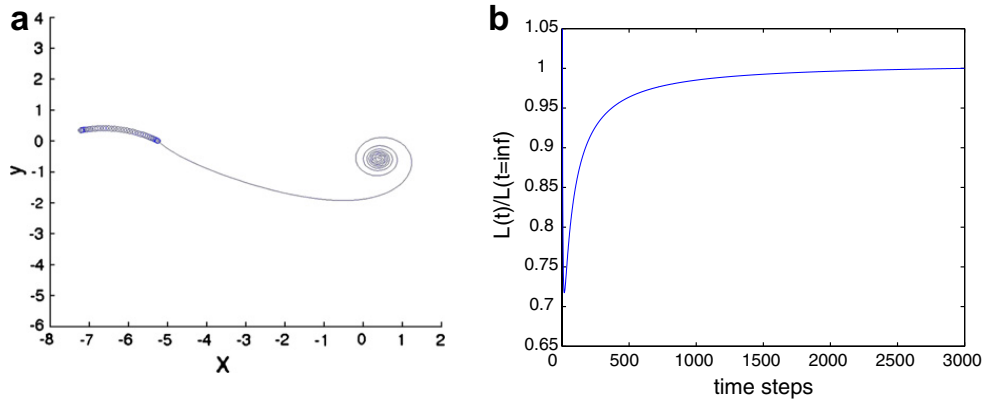

Fig. 15. (a) Heaviside Motion and (b) behavior of lift for a heaviside motion.

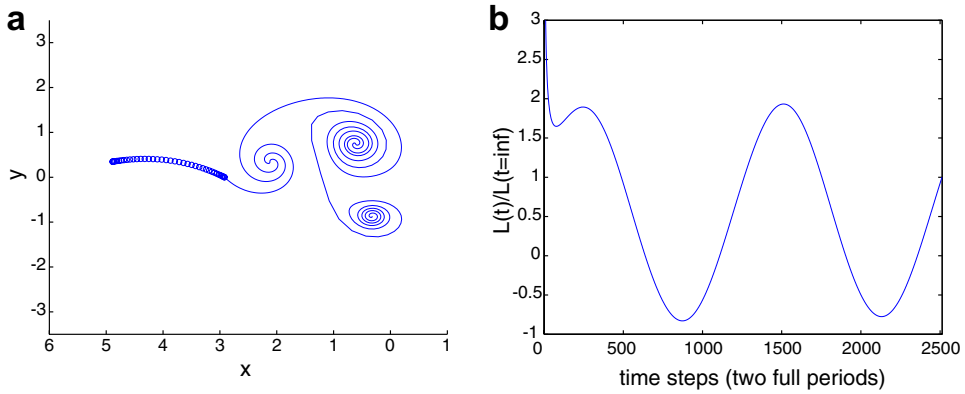

Fig. 16. (a) Fourier motion and (b) behavior of lift for a Fourier motion.

Because of the periodic motion, the lift will also show periodicity. The effective angle of attack will be given by the chord angle (10°) plus the angle due to the wing curvature. For $\epsilon_0 = 0.05$ the angle due to curvature varies between $\pm 5°$ which means that the effective angle of attack could be anywhere between around 15° and 5°. As a consequence, we expect to get lift during the motion. In Fig. 16b, it can be seen that the average lift is somewhere around 0.55 after two full periods.

8. Concluding remarks

The main objective of this paper was to get more insight into fish and bird locomotion. Even though the topic is incredibly vast, we tried to explain some features found in nature, such as the effect of the trailing wake on the thrust and lift. This was done using the new and efficient method of Wu which we demonstrated to be more reliable than the previous ones.

The new method can better capture the leading singular effect near the trailing edge, which improves the accuracy when dealing with some highly nonlinear movements. The vorticity blows up at the downstream edge of the starting vortex element, and the analytical analysis provided by our method succeeds in better resolving this issue. We showed that the present method is better than the other methods when verifying Wagner's result. We also discussed the convergence of the outer wake and were able to demonstrate that using a blob in Wu's method did not affect its accuracy, since the method is more dependent on the time step than on the blob size. All the results compared very well with the experiments available, and the method showed a great deal of robustness and accuracy over all the other models and simulations so far tested. When compared with Devenport's experiment, Wu's method gives a much better size of the vortex ring than the modified vortex blob method.

We began working on this project fascinated by Gray's paradox. He proved in 1936 that given the muscle power and the frictional drag experienced during the motion, a fish could not swim as fast as some of the species observed performing. One explanation for this might be the effect of the vortices released by the lateral fins on the tail fin. The tail fin could just take advantage of this vorticity present in the fluid and generate a greater thrust for the fish. Another unexplained fish behavior would be the extremely rapid U-turn a trout, for example, could make when approaching a wall at very high speed. All these examples involve extremely nonlinear motions and require some very fine mathematical analysis. We are hopeful that the new method presented in this paper can be used to capture these sensible details when dealing with highly-curved movements and wake-crossing maneuvers by highly deformable bodies with lifting-surfaces aptly appended.

References

[1] J.B. Bratt, Flow patterns in the wake of an oscillating airfoil, Aeronaut. Res. Council, R&M 1773 (1953).
[2] A.J. Chorin, P.S. Bernard, Discretization of a vortex sheet, with an example of roll-up, J. Comput. Phys. 13 (1973) 423–429.
[3] W.J. Devenport, M.C. Rife, S.I. Liapis, G.J. Follin, The structure and development of a wing-tip vortex, J. Fluid Mech. 312 (1996) 67–106.
[4] N. Didden, On the formation of vortex rings: rolling up and production of circulation, Z. Angew. Math. Phys. 30 (1979) 101–116.
[5] T.Y. Hou, V.G. Stredie, T.Y. Wu, A 3D numerical method for studying vortex formation behind a moving plate, Commun. Comp. Phys. 1 (2006) 206–227.
[6] K.D. Jones, C.M. Dohring, M.F. Platzer, Experimental and computational investigation of the Knoller–Betz effect, AIAA J. 36 (1998) 1240–1246.
[7] M.A. Jones, The separated flow of an inviscid fluid around a moving flat plate, J. Fluid Mech. 496 (2003) 405–441.
[8] von Th. Kármán, W.R. Sears, Airfoil theory for non-uniform motion, J. Aeronaut. Sci. 5 (1938) 6–17.
[9] J. Katz, A. Plotkin, Low-speed Aerodynamics, second ed., Cambridge University Press, 2001.
[10] M.M. Koochesfahani, Vortical patterns in the wake of an oscillating airfoil, AIAA J. 27 (1989) 1200–1205.
[11] R. Krasny, Vortex sheet computations: roll-up, wakes, separation, Lectures in Applied Mathematics, vol. 28, American Mathematical Society, 1991, pp. 385–402.
[12] J.C.S. Lai, J. Yue, M.F. Platzer, Control of backward-facing step flow using a flapping foil, Exp. Fluids 32 (2002) 44–54.
[13] M.J. Lighthill, Note on the swimming of slender fish, J. Fluid Mech. 9 (1960) 305–317.
[14] M.J. Lighthill, Aquatic animal propulsion of high hydromechanical efficiency, J. Fluid Mech. 44 (1970) 265–301.
[15] J.E. McCune, C.M.G. Lam, M.T. Scott, Nonlinear aerodynamics of two-dimensional airfoils in severe maneuver, AIAA J. 28 (1990) 385–393.
[16] D.W. Moore, The stability of an evolving two-dimensional vortex sheet, Mathematika 23 (1976) 35–44.
[17] N.I. Muskhelishvili, Singular integral equations; Boundary problems of function theory and their application to mathematical physics, Groningen, P. Noordhoff [c1953] 17 (1946) 23.
[18] J.N. Newman, The force on a slender fish-like body, J. Fluid Mech. 58 (1973) 689–702.
[19] J.N. Newman, T.Y. Wu, Unsteady flow around a slender fish-like body, IUTAM/ITTC Symposium on Direction Stability and Control of Bodies in Water, University College, London, 1972.
[20] J.N. Newman, T.Y. Wu, A generalized slender-body theory for fish-like forms, J. Fluid Mech. 57 (1973) 673–693.
[21] M. Nitsche, R. Krasny, Numerical study of vortex ring formation at the edge of a circular tube, J. Fluid Mech. 276 (1994) 139–161.
[22] D.I. Pullin, The large-scale structure of unsteady self-similar rolled-up vortex sheets, J. Fluid Mech. 88 (1978) 401–430.
[23] N. Rott, Diffraction of a weak shock with vortex generation, J. Fluid. Mech. 28 (1956) 111–128.
[24] P.G. Saffman, Vortex Dynamics, Cambridge University Press, 1992.
[25] T. Sarpkaya, Vortex element methods for flow simulation, Adv. Appl. Mech. 31 (1994) 113–247.
[26] V.G. Stredie, Mathematical Modeling and Simulation of Aquatic and Aerial Animal Locomotion, Ph.D. Thesis, California Institute of Technology, 2005.
[27] T. Theodorsen, General Theory of Aerodynamic Instability and the Mechanism of Flutter, National Advisory Committee for Aeronautics, Report No. 496, 1935.
[28] H. Wagner, Uber die Entstehung des dynamischer Auftrieb von Tragflugeln, Z.A.M.M. 5 (1925) 17–35.
[29] T.Y. Wu, Hydromechanics of swimming propulsion. III. Swimming and optimum movements of slender fish with side fins, J. Fluid Mech. 46 (1971) 545–568.
[30] T.Y. Wu, On theoretical modeling of aquatic and aerial animal locomotion, Adv. Appl. Mech. 38 (2001) 291–352.